Performance of AIRS ozone retrieval over the central Himalayas: Case studies of biomass burning, downward ozone transport and radiative forcing using long-term observations

Prajjwal Rawat[1,5], Manish Naja[1], Evan Fishbein[2], Pradeep K. Thapliyal[3], Rajesh Kumar[4], Piyush Bhardwaj[4], Aditya Jaiswal[1], Sugriva N. Tiwari[5], Sethuraman Venkataramani[6], Shyam Lal[6]

[1] Aryabhatta Research Institute of Observational Sciences (ARIES), Nainital, 263001, India
[2] NASA Jet Propulsion Laboratory, Pasadena, CA 91109, USA
[3] Space Applications Centre, ISRO, Ahmedabad 380015, India
[4] National Center for Atmospheric Research (NCAR) Boulder, CO 80307, USA
[5] DDU Gorakhpur University, Gorakhpur 273009, India
[6] Physical Research Laboratory (PRL), Ahmedabad, 380009, India

Corresponding author: Manish Naja (manish@aries.res.in)

Short Summary:

Satellite based ozone observations have gained wide importance due to their global coverage. However, satellite retrieved products are indirect and need to be validated, particularly over mountains. Here, ozonesondes launched from a Himalayan site are utilized to assess the AIRS ozone retrieval. AIRS is shown to overestimate ozone in the upper troposphere and lower stratosphere, while the differences with ozonesonde are lower in the middle troposphere and middle stratosphere.

Abstract

Data from 242 ozonesondes launched from ARIES Nainital (29.40^{o} N, 79.50^{o} E, and 1793 m elevation) are used to evaluate the Atmospheric Infrared Sounder (AIRS) version 6 ozone profiles and total column ozone during the period 2011-2017 over the central Himalaya. The AIRS ozone products are analyzed in terms of retrieval sensitivity, retrieval biases/errors, and ability to retrieve the natural variability of columnar ozone, which has not been done so far from the Himalayan region having complex topography. For a direct comparison, averaging kernels information is used to account for the sensitivity difference between the AIRS and ozonesonde data. We show that AIRS has lower differences with ozonesonde in the lower and middle troposphere and stratosphere with nominal underestimations of less than 20%. However, in the upper troposphere and lower stratosphere (UTLS), we observe a considerable overestimation of the magnitude, as high as 102%. The weighted statistical error analysis of AIRS ozone shows higher positive bias and standard deviation in the upper troposphere of about 65% and 25%, respectively. Similar to AIRS, Infrared Atmospheric Sounding Interferometer (IASI) and Cross-track Infrared Sounder (CrIS) are also able to produce ozone peak altitudes and gradients successfully. However, the statistical errors are again higher in the UTLS region that are likely related to larger variability of ozone, lower ozone partial pressure and inadequate retrieval information on the surface parameters. Furthermore, AIRS fails to capture the monthly variation of the total ozone column, with a strong bimodal variation, unlike unimodal variation seen in ozonesonde and Ozone Monitoring Instrument (OMI). In contrast, the UTLS and the tropospheric ozone columns are in reasonable agreement. Increases in the ozone values by 5 - 20% after biomass burning and during events of downward transport are captured well by AIRS. Ozone radiative forcing (RF) derived from total column ozone using ozonesondes data (4.86 mWm^{-2}) matches well with OMI (4.04 mWm^{-2}), while significant RF underestimation is seen in AIRS (2.96 mWm^{-2}). The fragile and complex landscapes of the Himalayas are more sensitive to global climate change and establishing such biases and error analysis of space-borne sensors will help study the long-term trends and estimate accurate radiative budgets.

1. Introduction

Atmospheric ozone is an essential trace gas that plays a crucial role in the atmospheric oxidizing chemistry, air quality, and earth's radiative budget. The stratospheric ozone absorbs harmful solar ultraviolet radiation and protects biological life on earth, whereas tropospheric ozone, being a secondary air pollutant (Logan et al., 1985; Pitts and Pitts, 1997; Pierce et al., 2009; Monks et al., 2015; Lelieveld et al., 2018) and greenhouse gas, contributes to global warming and can harm human health and crops when present in higher concentrations near the surface (Fishman et al., 1979; Ebi and McGregor 2008; Lal et al., 2017). Different radiative forcing of ozone from the stratosphere (cooling) to the troposphere (heating) (Lacis et al., 1990; Wang et al., 1993; Forster et al., 2007; Hegglin et al., 2015) demonstrate its potential importance as an atmospheric climate gas (Shindell et al., 2012; Thornhill et al., 2021). Hence, information regarding precise long-term variability in global ozone distribution is vital for better characterizing atmospheric chemistry and global climate changes (McPeters et al., 1994; Kim et al., 1996; Myhre et al., 2017).

In recent decades, observations of ozone from space-borne sensors (microwave limb sounding, UV-VIS, and IR) have become an increasingly robust tool for global and higher temporal monitoring (Fishman et al., 1986; Munro et al., 1998; Bhartia et al., 1996; Foret et al., 2014). This increases our ability to analyze various influences of human activities on the atmospheric chemical composition, including ozone, study their long-term impact on climate (Fishman et al., 1987; Fry et al., 2012; Tarasick et al., 2019; Thornhill et al., 2021), and estimate reliable radiative budgets (Hauglustaine and Brasseur 2001; Gauss et al., 2003; Aghedo et al., 2011). However, the space-based sensors are indirect and measure the atmospheric composition based upon specific algorithms utilizing radiative transfer models and a-priori information. Hence, the retrieval outputs

need to be evaluated with certain reference instruments for establishing the credibility and better utilization of space-borne data.

The Himalayas, a complex terrain region, has the largest abundance of ice sheets outside polar regions that impacts global/regional radiative budgets and climate pervasively (e.g., Lawrence and Lelieveld, 2010; Cristofanelli et al., 2014; Zhang et al., 2015). Very sparse in-situ and ground-based observations in this region, along with inadequate information on the surface parameters, makes it difficult to retrieve atmospheric composition from space-borne instruments. This is because the ozone weighting function, a measure of the retrieval sensitivity and a fundamental retrieval component, depends upon various atmospheric parameters like surface temperature, surface emissivity, and terrain height (Rodgers et al., 1976, 1990; Bai et al., 2014), which is not uniform over the foot-print size of the AIRS (~ 13 km x 13 km) over the Himalayas. Usually, the ozone weighting function has a shorter integrating path over the elevated terrain regions, which follows a smaller weighting function and provides lesser sensitivity and higher errors in the final retrievals (Coheur et al., 2005; Bai et al., 2014).

The Atmospheric Infrared Sounder (AIRS) onboard the Aqua satellite has been providing reliable vertical profiles of ozone, temperature, water vapor, and other trace gases globally twice a day since 2002. Numerous validation studies of AIRS retrieved ozone have been carried out for different versions since it started operating (2002). For example, Bian et al. (2007) studied AIRS version 4 over Beijing and discussed the potential agreements (within 10%) between AIRS and ozonesonde (GPSO3) ozone, particularly in the upper troposphere and lower stratosphere (UTLS) region with the capability of AIRS to identify various Stratosphere-Troposphere Exchange (STE)

and transient convective events. Similarly, a study over Boulder and Lauder by Monahan et al. (2007) using a similar AIRS version showed despite the larger biases in the lower and middle tropospheric region, the retrieval algorithm captures the ozone variability very effectively with a positive correlation of more than 70%. However, that study suggested a need for tropopause-adjusted coordinates in the a-priori profiles. Both these studies (Bian et al., 2007; Monahan et al., 2007) show larger biases in AIRS ozone in the lower and middle tropospheric regions; however, shifts in retrieval biases and errors were seen towards the UTLS region in version 5 (Divakarla et al., 2008), apart from significant improvements in the lower troposphere. The retrieval methodology has also changed significantly between V4 and V5. Version 4 or earlier used regression retrieval as the first guess in physical retrieval, while later versions used a climatology-based first guess for the physical retrieval based on other works (McPeters et al., 2007). Also, radiative transfer models, selected channel sets, and clarified quality indicators have been modified and improved in all successive versions.

The AIRS ozone retrieval in V5 has improved significantly with retrieval biases and root mean square error (RMSE) less than 5% and 20%, respectively (Divakarla et al., 2008), over the tropical regions. However, there is not much discussion and studies of the assessment for AIRS ozone over the Himalayas' complex terrain, where retrieval is expected to be erroneous due to large surface variability within its footprint. Also, most of the previous studies (Bian et al., 2007; Divakarla et al., 2008; Pittman et al., 2009) did not utilize the averaging kernels information of the AIRS that is vital for satellite evaluation.

Here, the evaluation of AIRS version 6, which entirely depends upon the infra-red (IR) observations after the failure of the AMSU sensor, is presented in terms of statistical analysis and ability to retrieve the natural variability of ozone at various altitudes over the central Himalayan region using in-situ ozonesonde observations convolved with AIRS averaging kernels. Additionally, the present study assessed the AIRS retrieval algorithm using IASI and CrIS radiance information for one year. AIRS columnar ozone (i.e., total, UTLS, and tropospheric columns) is also assessed with ozonesonde, OMI, and Microwave Limb Sounder (MLS) observations. AIRS has a long-term data set for ozone and meteorological parameters, establishing such biases and error analysis is essential to make meaningful use of its data to characterize the Himalayan atmosphere, study the trends, radiative budgets, perform the model evaluation and data assimilation over this region.

2 Data and Methodology

2.1 Data Description

2.1.1 AIRS

Atmospheric Infrared Sounder (AIRS) onboard Aqua satellite, in the sun synchronous polar orbit at 705 km altitude, is a hyperspectral thermal infrared grating spectrometer with equatorial crossings at ~13:30 local time (LT). It is a nadir scanning sensor that was deployed in orbit on May 4, 2002. AIRS, along with its partner microwave instrument, the Advanced Microwave Sounding Unit (AMSU-A), represents the most advanced atmospheric sounding system placed in space using cutting-edge infrared and microwave technologies. These instruments together observe the global energy cycles, water cycles, climate variations, and greenhouse gases, however, after AMSU failure, the retrieval now mostly depends upon the AIRS IR observations. The AIRS

infrared spectrometer acquires 2378 spectral samples at resolutions ($\lambda/\Delta\lambda$) ranging from 1086 to 1570 cm^{-1}, in three bands: 3.74 µm to 4.61 µm, 6.20 µm to 8.22 µm, and 8.8 µm to 15.4 µm (Fishbein et al., 2003; Pagano et al., 2003). The independent channels of AIRS permit retrieval of various atmospheric states and constituents depending upon their corresponding spectral response, even in the presence of a 90% cloud fraction (Susskind et al., 2003; Maddy and Barnet, 2008). In this study, we have used Level 2 Support physical products of AIRS (AIRS2SUP). The AIRS2SUP files (~240 granules/day) possess extra information over the standard AIRS files, e.g., information on averaging kernel and degree of freedom, including vertical profiles at 100 pressure levels, against just 28 in the standard product.

The support product profiles contain 100 levels between 1100 and 0.016 mbar. While it has a higher vertical resolution, the vertical information content is no greater than the standard product. The information on averaging kernels and degree of freedoms (DOFs) is utilized to understand the retrieved products more comprehensively. The DOFs of ozone, a measure of significant eigen functions used in the AIRS retrieval, have an average value of 1.36 over the tropical latitude band (Maddy and Barnet 2008) (Table S1), while over the balloon collocated region, an average DOFs of 1.62 is observed (Figure S1). In the present study, the AIRS data is flagged as best quality when the cloud fraction is less than 80%, and the degrees of freedom (DOF) are greater than 0.04. However, analysis of cloud fraction over our collocated region shows (Figure S2) only 7% of observations during 2011 - 2017 had a cloud fraction of more than 80%.

2.1.2 IASI (NOAA/CLASS)

The Infrared Atmospheric Sounding Interferometer (IASI) onboard MetOp satellites, with a primary focus on meteorology than climate and atmospheric chemistry monitoring, is a nadir viewing Michelson interferometer (Clerbaux et al., 2007). The first MetOp satellite was launched in October 2006 (MetOp-A), and IASI was declared operational in July 2007. MetOp is a polar sun-synchronous satellite having descend and ascend nodes at 09:30 and 21:30 LT, respectively. IASI measures in the IR part of the EM spectrum at a horizontal resolution of 12 km at nadir up to 40 km over a swath width of about 2,200 km. IASI covers an infra-red spectral range between 3.7 to 15.4 μm with a total of 8461 spectral channels, out of which 53 channels around 9.6 μm are utilized for ozone retrieval. IASI level 2 ozone products provided by NOAA National Environmental Satellite Data and Information Service (NESDIS) Center for Satellite Application and Research (STAR) are used in this study. The IASI (NOAA/CLASS) ozone product is retrieved based on the AIRS algorithm and has various quality control flags (Table S2). Only QC=0 data which represents a successful IR ozone retrieval, is used.

2.1.3 CrIS/ATMS (NUCAPS)

The Cross-track Infrared Sounder (CrIS) and Advanced Technology Microwave Sounder (ATMS) onboard the Suomi NPP satellite were launched in 2011 to feature the high spectral-resolution ("hyperspectral") observations of earth's atmosphere. The CrIS instrument is an advanced Fourier transform spectrometer with an ascending node 13:30 LT and flies at a mean altitude of 824 km and performs fourteen orbits per day. It measures high-resolution IR spectra in the spectral range 650 - 2550 cm^{-1} with a total of 1305 channels. The ATMS is a microwave sounder with a total of 22 channels ranging from 23 to 183 GHz. These two instruments, CrIS and ATMS, operate in an

overlapping field-of-view (FOV) formation, with ATMS FOVs re-sampled to match the location and size of the 3×3 CrIS FOVs for retrieval under clear to partly cloudy conditions. Here the NUCAPS algorithm-based ozone product of CrIS is utilized. The NOAA Unique CrIS/ATMS Processing System (NUCAPS) is a heritage algorithm developed by the STAR team based on the AIRS retrieval algorithm (Susskind et al., 2003, 2006). The NOAA implemented NUCAPS algorithm is a modular architecture that was specifically designed to be compatible with multiple instruments. The same retrieval algorithms are currently used to process the AIRS/AMSU suite (operations since 2002), the IASI/AMSU/MHS suite (operational since 2008), and now the CrIS/ATMS suite (approved for operations in January 2013). Here again, various quality controls for retrieved data are provided by the NUCAPS science algorithm team, and we used QC=0 for lesser discrepancies in our evaluation (Table S2). These research products follow a similar retrieval algorithm as developed by the AIRS science team, which gives us further opportunity to assess the AIRS retrieval algorithm for IASI and CrIS radiances.

2.1.4 Ozonesonde

EN-SCI electrochemical concentration cell (ECC) ozonesondes and GPS-radiosondes (iMet) have been launched from the Aryabhatta Research Institute of Observational Sciences (ARIES) (29.4^{o} N, 79.5^{o} E, and 1793 m elevation) Nainital (Figure 1), a high-altitude site in central Himalaya, since 2011 (Ojha et al., 2014; Rawat et al., 2020), the only facility in the Himalayan region having regular launchings. ECC ozonesonde relies on the oxidation reaction of ozone with potassium iodide (KI) solution (Komhyr et al., 1967, 1995) to measure ozone partial pressure in the ambient atmosphere. The typical vertical resolution of ozonesonde is about 100 - 150 m and has a precision of better than ± 3 - 5 % with an accuracy of about ± 5 - 10 % up to 30 km altitude under standard

operating procedures (Smit et al., 2007; Smit & ASOPOS Panel, 2020). The ozonesonde is connected to iMet-radiosonde via a V7 electronic interface, where radiosonde consists of GPS, PTU, and a transmitter to transmit signals to the ground. The ozonesonde sensor's successful performance is assured before launch (about 3 - 7 days before launch) as part of advance preparation and during the day of launch by maintaining and reviewing the records for background current, pump flow rate, response time, etc. The ozonesonde data quality is further assured by estimating these ECC ozonesondes' total ozone normalization factor with collocated OMI total ozone. These factors are well within the ASOPOS recommendation with an average of 1.0 ± 0.04, which implies the reasonable quality of these ozonesondes (Smit & ASOPOS Panel, 2020). Additionally, ozonesonde observations from present site have also been utilized in SUSKAT (Bhardwaj et al., 2018) and StratoClim (Brunamonti et al., 2018) field campaigns and in other studies (Ojha et al., 2014). Further, owing to higher accuracy and in-situ measurement, ozonesonde has been widely used worldwide for satellite and model validation (Divakarla et al., 2008; Nassar et al., 2008; Monahan et al., 2007; Kumar et al., 2012a, 2012b; Dufour et al., 2012; Verstraeten et al., 2013; Boynard et al., 2016; Rawat et al., 2020). Both the ascending and descending data were recorded by ozonesonde, however, due to time lag in descending records, only ascending data is utilized (Lal et al., 2013, 2014; Ojha et al., 2014). The data is collected at the interval of about 10 meters which is averaged over 100 meters interval using a 3σ filter that removes the outlier values (Srivastava et al., 2015; Naja et al., 2016).

2.1.5 Other Auxiliary Data

Additionally, collocated and concurrent OMI and MLS observations are also used to study the tropospheric ozone, UTLS, and total ozone column due to their reasonable sensitivity and well-

validated retrievals (Veefkind et al., 2006; Ziemke et al., 2006; Fadnavis et al., 2014; Wang et al., 2021). The tropospheric ozone column obtained from OMI and MLS is based on the residual method, which depends upon the collocated difference between the MLS stratospheric ozone column and OMI total ozone column, which is described in detail by Ziemke et al. (2006). Furthermore, the MLS version 4 data is utilized for the UTLS column above 261 hPa due to its credibility in this range for scientific applications (Livesey et al., 2013; Schwartz et al., 2015). Moreover, for fair statistical analysis between ozonesonde and MLS ozone profile, Gaussian smoothing is applied to ozonesonde with full width at half maximum equal to typical upper tropospheric vertical resolution (~ 2 - 4 km) of MLS (Livesey et al., 2013). The best quality data of MLS with data flags, i.e., status=even, quality > 0.6, and convergence < 1.18, is utilized (Ziemke et al., 1998; Barre et al., 2012). However, a slightly different collocation criterion of $3^o \times 3^o$ grid box and daytime collocation is utilized for MLS in this work due to coarser resolution and to get sufficient matchups.

2.2 Methods of Analysis

The balloon launch time is mostly around 12:00 IST (Indian Standard Time, which is 5.5 hours ahead of GMT). The Aqua satellite comes over the India around 1:30 pm and 1:30 am IST. Hence for collocation, only noontime (ascending) data (or ± 3 hours of balloon launch) with $1^o \times 1^o$ spatial collocation were chosen in this evaluation. However, for some days, there was no noontime granule in AIRS retrieval (nearly 35 out of total 242 soundings), then we used a loose collocation of ±1 day. However, no significant changes were seen after such flexible collocation. Most of the ozonesondes have burst altitudes near 10 hPa, hence AIRS ozone profiles are evaluated from surface to 10 hPa.

Although suitable collocation criteria have been defined for a fair comparison, still different vertical resolutions of the two data sets (ozonesonde ~100 m and AIRS ~1-5 km) make the meaningful comparison difficult (Maddy and Barnet, 2008; Verstraeten et al., 2013; Boynard et al., 2016). The difference in vertical resolution and retrieval sensitivity must be accounted for a meaningful comparison. Though there is no perfect way to remove the error arising from the different vertical resolutions of the two measurements, still utilizing the averaging kernel smoothing or Gaussian smoothing, the error is minimized. Various groups have used the satellite averaging kernels smoothing to compare satellite measurements with ozonesonde (Zhang et al., 2010; Verstraeten et al., 2013; Boynard et al., 2016, 2018), while Gaussian smoothing (Wang et al., 2020) and broad layer columns (Nalli et al., 2017) are also utilized. In the present analysis, averaging kernel smoothing is utilized. First, ozonesonde data were interpolated at all AIRS Radiative Transfer Algorithm (RTA) layers from surface to burst altitude, then ozonesonde profiles were smoothed according to the AIRS averaging kernel and a-priori profile (ML climatology), leading to a vertical profile [ozonesonde (AK)] representing what AIRS would have measured for the same ozonesonde sampled atmospheric air mass in the absence of any other error affecting satellite observations. According to Rodgers and Connor (2003), the smoothing of the true state can be characterized as follows:

$$X_{est} = X_0 + A' (X_{sonde} - X_0) \qquad (1)$$

The AIRS provides averaging kernels information at 9 pressure levels (Figure 2b) whereas the AIRS RTA has 100 pressure levels. So following ozone vertices (Table S3) and formulating trapezoid matrix (Figure 2a, the details regarding the calculation of trapezoid matrices are given in AIRS/AMSU/HSB Version 6 Level 2 Product Levels, Layers and Trapezoids), we convert 9 levels AIRS averaging kernels to 100 levels averaging kernels using following defined operation.

311 $$A' = F \times A_{trapezoid} \times F' \qquad (2)$$

312 Where $A_{trapezoid}$ and F are averaging kernel matrices and trapezoid matrices (F' is pseudo-inverse
313 of F). $A_{trapezoid}$ is a given product, while F is calculated for given ozone vertices (Table S3).

314 Further, in the thermal IR spectrum, the contribution of ozone or any other trace gas towards
315 emission/absorption of IR radiation in the radiative transfer equation depends on the exponent of
316 layer integrated column amounts (Maddy and Barnet, 2008). Hence logarithmic changes in layer
317 column density are more linear than absolute changes. So logarithmic equations are used instead
318 of Eq. 1 for smoothing ozonesonde data in the present study.

319 $$\ln(X_{est}) = \ln(X_0) + A'\{\ln(X_{sonde}) - \ln(X_0)\} \qquad (3)$$

320 Where X_{est}, X_{sonde}, and X_0 are smooth ozonesonde or ozonesonde (AK), true ozonesonde, and first
321 guess (ML climatology) profiles, respectively. Knowing the nature of convolution from Eq. 1 and
322 3, it can be observed that the ozonesonde (AK) or smooth ozonesonde will have more weights
323 toward a-priori profiles when satellite retrieval is poor or AKs approaches zero values.

324 More details on the calculation of averaging kernels can be found in AIRS documents
325 (AIRS/AMSU/HSB Version 6 Level 2 Product Levels, Layers and Trapezoids) or in available
326 literature (Maddy and Barnet, 2008; Irion et al., 2018). A typical averaging kernels matrix and
327 other parameters are shown in Figure 2. Figure 2a shows a typical trapezoid matrix, Figure 2b
328 shows the averaging kernels at 9 pressure levels, Figure 2c shows constructed averaging kernels
329 at 100 RTA layers, and Figure 2d shows an example of the different ozone profiles convolved with
330 AKs on 15 June 2011 over the observation site.

331

2.3 Statistical Analysis

The error analysis for AIRS retrieval with interpolated and smoothed ozonesonde is based on Nalli et al. (2013, 2017). Bias, root mean squared error (RMSE), and standard deviation (STD) are studied at various RTA vertical levels from the surface to 10hPa over the Himalayan region. The finer spatio-temporal collocation utilized here has further minimized the uncertainty and error in the evaluation. Since the observation site (29.4^o N, 79.5^o E) is at a latitude lower than 45^o; hence there is a lesser overlap of satellite passes, and mostly a few nadir scans are close to the observation site (mostly daytime granules in the range of 75 to 85). Hence all the daytime observations of AIRS are close to ± 3 hours of temporal collocation to the ozonesonde launch and possess a lesser chance of time mismatch.

Given the collocated ozone mixing ratio profiles for satellite, ozonesonde (AK), and in-situ truth (ozonesonde) observations, the statistical errors are calculated as follows -

$$\text{RMSE } (\Delta O_l) = \sqrt{\frac{\sum_{j=1}^{j=n} W_{l,j} \times (\Delta O_{l,j})^2}{\sum_{j=1}^{j=n} W_{l,j}}} \qquad (4)$$

$$\text{Bias } (\Delta O_l) = \frac{\sum_{j=1}^{j=n} W_{l,j} \times (\Delta O_{l,j})}{\sum_{j=1}^{j=n} W_{l,j}} \qquad (5)$$

Here *l* runs over different RTA layers and j runs for all collocated profiles, $\Delta O_{l,j}$ the fractional deviation is taken to be the absolute deviation divided by the observed value. Where $\Delta O_{l,j} = \left(\frac{O^R{}_{l,j} - O^T{}_{l,j}}{O^T{}_{l,j}}\right)$, O^T and O^R are ozonesonde/ozonesonde (AK) and satellite retrieved ozone mixing ratio, respectively. $W_{l,j}$ is the weighting factor and assumes one of three forms $W_0 = 1$, $W_1 = O^R$ and W_2

$= (O^R)^2$ and for ozone to minimize skewing impact due to large variation in mixing ratio at different altitudes, we have used the W_2 weight factor as suggested by other sounder science team (Nalli et al., 2013, 2017). The Standard deviation (STD) is then calculated by the square root of difference between RMSE and biases square at different RTA levels. Further to check the strength of the linear relationship between the satellites retrieved data and ozonesonde data the square of Pearson's correlation coefficient is also calculated.

2.4 Estimation of Columnar Ozone

The total column ozone (TCO) from ozonesonde is calculated by integrating the ozone mixing ratio from the surface to burst altitude and then adding residual ozone above burst altitude. Here the residual ozone is obtained from satellite-derived balloon-burst climatology (BBC) (McPeters and Labow, 2012; Stauffer et al., 2022). The discrete integration for calculation of total ozone column (DU) between defined boundaries is performed as follows:

$$\text{Total column ozone} = 10^7 \times \left(\frac{RT_o}{g_o P_o}\right) \times \sum_{j=1}^{j=n} 0.5 \times (VMR[i] + VMR[i+1]) \times (P[i] - P[i+1]) \quad (6)$$

Where P is ambient pressure in hPa, VMR volume mixing ratio of ozone in ppbv, R (= 287.3 $JKg^{-1}K^{-1}$) gas constant, g_o (= 9.88 ms^{-2}), P_o (= 1.01325×10^5 Pa) and T_o (= 273.1 K) standard temperature.

The UTLS ozone column (DU) is also calculated using Eq. (6), where the UTLS region is defined between 400 hPa to 70 hPa (Bian et al., 2007). Additionally, the tropospheric ozone column (DU) is calculated for ozonesonde utilizing Eq. (6) with boundaries from the surface to the lapse rate tropopause (LRT). The tropopause height from balloon-borne observations is estimated using the lapse rate method as well as the AIRS-derived tropopause is used and shown in Figure 3. However,

for OMI and MLS tropospheric ozone residual method is used, which calculates the tropospheric ozone column by subtracting the OMI total column from MLS stratospheric ozone column (Hudson et al., 1998; Ziemke et al., 2006).

3. Results and Discussion

3.1 Ozone Distribution along Balloon Trajectory: Ozonesonde and AIRS

The distributions of ozone along the balloon tracks obtained using all ozone soundings data during four seasons are shown in Figure 4. The nearest swath of AIRS ozone observations is interpolated to the balloon locations and altitudes. Altitude variations of the balloon along longitude are shown in Figure S3. The balloons drift to a very long-distance during winter, followed by autumn and spring. During these seasons, balloons often reach Nepal also. The wind reversal took place during the summer-monsoon when the balloon drifts towards IGP regions (Figure 4). The distributions of ozone from AIRS are more-or-less similar to the distributions those from ozonesonde. Here, the ozone variations are reflecting in terms of spatial as well as vertical distributions. The bias and coefficient of determination (r^2) between ozonesonde and AIRS ozone are studied along the longitude and latitude (Figures S3 and S4). Lower biases (lesser than 10%) and higher r^2 are seen in the lower and middle troposphere. The poor correlation (<0.4) and larger biases of up to 28% are seen at certain longitudes that are associated with higher altitudes (> 20 km). Around the balloon launch site (Nainital, 79.45^o E) highest r^2 score of 0.98 and low bias of 1.4% are observed, which remain higher (r^2) and lower (bias) up to 80^o E (Figure S3).

3.2 Ozone Soundings and AIRS Ozone Profiles

Figure 5 shows the average monthly ozone profiles for collocated observations of ozonesonde and AIRS, respectively, during seven-year periods. The ozonesonde convolved with AIRS averaging kernels [ozonesonde (AK)] and AIRS a-priori are also compared. The value of percentage difference between ozonesonde (AK) and AIRS ozone at 706, 617, 496, 103, 29, and 14 hPa altitudes are shown in figure 5, and the zoomed variations in the lower tropospheric ozone (surface to 200 hPa) are also presented in the insets. AIRS slightly (~10%) underestimates ozone in the lower troposphere during most of the months, except the summer-monsoon (June-August), where an overestimation of up to 20% is observed. In the middle troposphere, around 300 hPa, an underestimation in the range of 1 - 17% is seen for all months with an approaching tendency of ozonesonde (AK) towards the true ozonesonde profiles. However, near the tropopause region, AIRS retrievals considerably overestimate ozone by up to 102%. The overestimation was highest for the winter season (82 - 102%), followed by the spring, and autumn, while lowest for the summer-monsoon season (10 - 27%). In the stratosphere, where the sensitivity of AIRS is higher (Figure 2c), the ozonesonde and AIRS differences were relatively lesser. Additionally, AIRS retrieval shows an underestimation of 5 - 21% in this altitude region.

As expected, the difference between ozonesonde and AIRS is significantly reduced (Table 1) after applying the averaging kernel or accounting for the sensitivity difference. This reduction was more notable for the summer monsoon period near the tropopause, where the difference reduced from 92% to 19%, providing an improvement of 72%. The improvement was as high as 100% on a monthly basis. Additionally, relative difference profiles were also analyzed for individual soundings as well for the different seasons (Figure S5). Higher differences of about 150% between

AIRS and ozonesonde ozone observations were seen in the upper troposphere and lower stratospheric (UTLS) region. The higher difference during winter and spring between these observations in the UTLS region could be due to recurring ozone transport via tropopause folding over the observation site. Such events may remain undetected by AIRS due to lower vertical resolution leading to the missing of some tropopause folding events at lower altitudes (Figure 3). However, in the lower troposphere, larger differences between ozonesonde and AIRS during summer-monsoon are seen, which are due to low ozone and frequent cloudy conditions leading to poor retrieval. The arrival of cleaner oceanic air during the south-west monsoon (or summer monsoon) brings ozone-poor air and frequent cloudy conditions over northern India that weakens the photochemical ozone production (Naja et al., 2014; Sarangi et al., 2014). Moreover, in the lower troposphere, the limited sensitivity of hyperspectral satellite instruments has a significant contribution from the a-priori information, which is also observed for AIRS retrieval (Figure 5).

Figure 6 shows the yearly time series analysis of the average ozone mixing ratio at four defined layers, characterizing the middle troposphere (600 - 300 hPa), the upper troposphere (300 - 100 hPa), lower stratosphere (100 - 50 hPa), and middle stratosphere (50 - 10 hPa) respectively. A prominent seasonality was seen in the time series throughout the years, which is quite clear in the upper troposphere (300 - 100 hPa). The ozone seasonality contrast reflects the influence of summer-monsoon and winter seasons. The seasonality contrast is similar between AIRS and ozonesonde measurements, while a reversal of ozone seasonality is observed in the middle stratospheric region compared to other layers. The opposite seasonality of the middle stratospheric region is primarily due to dominant circulations, variation of solar radiation and dynamics. Total

444 column water vapor is also shown in Figure 6 that shows a tendency of anti-correlation with ozone
445 in the 300 - 100 hPa region.
446
447 We have also estimated the monsoon index by the difference between zonal (U) wind (MERRA-
448 2 reanalysis data) at 850 hPa over the Arabian Sea (40^o E - 80^o E, 5^oN - 15^o N) and over the central
449 Indian landmass (70^o E - 90^o E, 20^o N - 30^o N) as done by Wang et al. (2001).
450 In general, the positive values of the monsoon index correspond to strong monsoons and negative
451 values correspond to weak monsoon periods (Wang et al., 2001). During the weak monsoon, there
452 is relatively drier air, lower cloud cover and higher surface temperature compared to the strong
453 monsoon period (Lu et al., 2018). We observed a tendency of lower annual average ozone (from
454 ozonesonde and AIRS measurements) during greater (positive) monsoon index and higher annual
455 average ozone during lower (negative) monsoon index. Lu et al. (2018) have shown an anti-
456 correlation (0.46) of tropospheric ozone with monsoon index over the Indian region. The years
457 2011, 2012, 2014, and 2015 are classified as weak monsoon years and relatively higher ozone is
458 seen during these years, whereas for the years 2013, 2016, and 2017, strong monsoon is observed,
459 and average yearly ozone was lesser during these years (Figure 6 bottom left). The relative
460 difference of AIRS ozone with ozonesonde in the upper tropospheric region also shows an anti-
461 correlation (Figure 6) of 0.17 with total column water vapor. Furthermore, the larger ozone
462 differences between AIRS and ozonesonde are associated with the lower water vapor (Figure S6),
463 which may be arising due to the influence of ozone-sensitive water vapor (WV) channels in mid-
464 Infra-red regions. Further, in the middle troposphere (600-300 hPa), a secondary ozone peak in
465 post-monsoon is observed, which is suggested to be influenced by the biomass burning (Figure
466 S7) over northern India that seems to be missing in the AIRS ozone.

In the middle troposphere (600 - 300 hPa) and lower stratosphere (100 - 50 hPa), AIRS retrievals show higher differences with respect to ozonesondes, while a nominal difference is observed for the middle troposphere and middle stratosphere (Figure S6). Furthermore, a systematic increase in standard deviation is also seen with the altitude. The higher standard deviations in the upper tropospheric and stratospheric regions are mainly due to higher ozone variability associated with stratosphere-troposphere exchange (STE) processes over the Himalayan region (Naja et al., 2016; Bhardwaj et al., 2018).

3.3 Statistical Analysis of AIRS Ozone Profiles

Error analysis of AIRS retrieved ozone over the Himalayan region is performed with spatio-temporal collocated ozonesonde observations as a reference. The methodology to calculate the root mean square error (RMSE), bias, and standard deviation (STD) is described in section 2.3. W_2 weighting statistics are utilized due to abrupt changes in atmospheric ozone with altitude. Here bias and STD between AIRS and ozonesonde are calculated at different RTA layers from surface to 10 hPa. Figure 7 shows the average variation of bias and STD at different RTA layers from surface to 10 hPa over this region. The mean biases between ozonesonde and MLS, a high vertical resolution satellite instrument, are also shown in figure 7. In general, higher positive biases (~65%) and STDs (~25%) in AIRS ozone retrieval are seen in the UTLS region, where MLS agrees well with ozonesonde. In the lower and middle troposphere, the AIRS ozone retrieval is negatively biased (0 - 25%), which increases gradually from the surface to higher altitudes (~ 350 hPa). A negative bias was also seen in the stratosphere of about 15%. Similar to the biases, STDs are also smaller in the lower troposphere and stratosphere, with values of nearly 15%. The higher statistical

errors in the upper troposphere and the lower stratospheric region could be due to lower ozone partial pressure and frequent stratospheric to tropospheric transport events over the Himalayas (Rawat et al., 2020, 2021), which introduces errors either after a mismatch of events in AIRS coarser vertical resolution or due to complex topography. Additionally, the AIRS tropopause frequency distribution shows less ability of AIRS to capture deep intrusion events (Figure 3). Further, AIRS trace gas retrieval largely depends on successful temperature retrieval and uses temperature retrieval as an input parameter (Maddy and Barnet, 2008). Hence, temperature retrieval error could also propagate to ozone, and statistical error analysis of AIRS temperature shows relatively higher biases (~ 2 K) in the upper tropospheric region (Figure S8).

The statistical error analysis was more-or-less similar for both true and smoothed ozonesonde profiles. However, notable reduction in tropospheric bias and vertical shifts of errors were also observed after applying the averaging kernel matrix to the true ozonesonde throughout the profile. A shift of the error peak is seen from the lower stratosphere to the upper troposphere. This could be due to the higher sensitivity of AIRS retrieval in the lower stratosphere, which would have minimized the error at these particular altitudes. However, in the upper troposphere, higher contribution of a-priories, as well as other factors (i.e., STE), might have resulted in larger biases and errors.

The histogram of differences between AIRS and ozonesonde (AK) is also studied at four defined layers (Figure 8). AIRS mostly underestimated ozone with a mean bias of 2.37 ppbv, 9.29 ppbv, and 39.8 ppbv in 800 - 600 hPa, 600 - 300 hPa, and 100 - 50 hPa layers, respectively, while in the upper troposphere (300 - 100 hPa) AIRS overestimated with a mean bias of 43.22 ppbv.

Furthermore, distributions of differences are skewed toward the negative values in the lower stratosphere and towards positive values in the upper troposphere. A more symmetric distribution over the negative axis is observed in the middle and lower troposphere. We also studied the correlation profiles for different seasons (Figure 8, right panel). A strong correlation is seen in the lower and middle troposphere for spring and summer, while there is a poor correlation for winter and autumn. In the lower troposphere, a larger difference between AIRS and ozonesonde (AK) is observed, particularly during summer, with a relatively higher correlation mostly due to the greater concurrence of AIRS a-priori with ozonesonde (AK). Whereas, in the upper troposphere (300 - 100 hPa), a larger difference during winter and spring is primarily due to frequent subtropical dynamics, while a higher correlation during the winter is mainly contributed from the AIRS retrieval. Furthermore, analysis of the correlation coefficient between AIRS and ozonesonde over different regions shows a higher correlation in the middle stratosphere (0.95) and lower stratosphere (0.92), followed by upper troposphere (0.68), lower troposphere (0.62), and middle troposphere (0.47).

3.4 Assessment of AIRS Retrieval Algorithm with IASI and CrIS Radiance

The MetOp/IASI and Soumi-NPP/CrIS radiance-based ozone products are assessed using ozonesonde data over the central Himalayan region for one year (April 2014 to April 2015), utilizing a total of 32 soundings. Here, the IASI and CrIS based ozone retrievals are research products provided by NOAA, whose retrieval is based on the AIRS retrieval algorithm and follows a similar averaging kernels matrix (Nalli et al., 2017). For IASI, due to the 09:30 ascending nodes (morning overpass in India), ±6 h loose temporal collocation is used. However, CrIS and AIRS follow the same collocation due to a similar noontime overpass. The IASI, CrIS, and AIRS sensors

have 8461, 1305, and 2378 IR channels, respectively. Hence, analyzing their satellite ozone products further helps to assess the AIRS retrieval algorithm for different IR radiances and channel sets.

Figure 9a shows the seasonal ozone profiles obtained from three IR satellite sensors along with ozonesonde for one year period. All sensors showed more-or-less similar ozone peak altitude and ozone gradient. The estimated ozone peak altitude for ozonesonde, AIRS, IASI, and CrIS are 11.35 hPa, 10 hPa, 9.11 hPa, and 7.78 hPa, respectively. The estimated average ozone gradient in regions between tropopause to gradient peak are 231.5 ppbv/hPa, 199.0 ppbv/hPa, 193.2 ppbv/hPa, and 199.1 ppbv/hPa for ozonesonde, AIRS, CrIS, and IASI, respectively.

Moreover, the higher ozone values during spring throughout the troposphere are captured well by all satellite sensors. Higher ozone during spring and winter in the UTLS region is observed well by AIRS and IASI, similar to ozonesonde but such features seem to be missing in CrIS ozone retrieval. At the same time, CrIS sensitivity looks relatively low, where the possible role of the number of channels can be seen. However, IASI and AIRS have effectively captured the ozone seasonal variability.

Figure 9b shows the weighted statistical error analysis of IASI, CrIS, and AIRS ozone retrieval with the true ozonesonde observations. Here, the difference in sensitivity of the two data sets is not accounted for as this section's primary aim is to assess the AIRS retrieved algorithm using different IR sensor radiances and channel sets. All three space-borne sensors overestimated UTLS ozone by more than 50%, however, in the stratosphere and lower troposphere, the bias was slightly

lower, and it is somewhat underestimated. Similar to bias, the STDs were also higher in the UTLS region by more than 60%. A consistent larger differences in the UTLS region for all three IR satellite sensors that share the similar radiative transfer model and retrieval algorithm shows the possible influence of complex topography and the various STE processes, in introducing errors in retrieval processes, apart from input a-priories of the retrieval.

Additionally, Pearson correlations between ozonesonde and IASI, CrIS, and AIRS are also studied at five atmospheric layers (i.e., 600 - 800 hPa, 300 - 600 hPa, 100 - 300 hPa, 50 -100 hPa, and 10 - 50 hPa) (Table 2). A relatively stronger positive correlation is found in the middle stratosphere (50 - 100 hPa) and lower stratosphere (50 - 100 hPa), which was highest for AIRS, followed by CrIS and IASI, and a relatively low correlation is observed in the middle troposphere (300 - 600 hPa) for AIRS and IASI (~ 44% and 31%), while CrIS shows the poorest correlation in the lower troposphere about 9%. The lower concurrence between ozonesonde and the satellite sensors in the lower troposphere could be due to lower sensitivity and shorter lifetime of near-surface ozone that could increase the a-priori contribution and sampling mismatch, respectively.

3.5 Columnar Ozone

3.5.1 Total Column Ozone (TCO)

Figure 10a shows variations in monthly average total column ozone (TCO) from ozonesonde, AIRS, and OMI during 2011 - 2017. Here the box plots are also overlaid on the mean column to describe the distribution of monthly column data. In general, the TCO is higher during spring, which subsequently drops in summer-monsoon. AIRS TCO shows a bimodal monthly variation which is not seen in the ozonesonde and OMI observations, otherwise, its monthly variation is in

582 reasonable agreement with ozonesonde. The OMI TCO is in a good match with the ozonesonde
583 with a maximum difference of up to about 5 DU. Table 3 shows the difference in the TCO between
584 AIRS, OMI, and ozonesonde. AIRS shows considerable overestimation in the range of 2.2 - 22
585 DU for some months while notable underestimation (1.8 - 4 DU) for others, with respect to both
586 ozonesonde and OMI. The correlation between AIRS TCO and ozonesonde TCO is found to be
587 0.5 (Table S4). To further understand the cause of bimodal variations in AIRS (higher ozone during
588 August, September, and October), the AIRS ozone profiles were integrated between different
589 stratospheric regions (100 - 70 hPa, 70 - 50 hPa, 50 - 20 hPa, and 20 - 1 hPa) and we found that
590 the elevated total ozone during post-monsoon is mainly contributed from the altitude above 50
591 hPa.
592
593 **3.5.2 UTLS Ozone Column**
594 Figure 10b shows the variations in the monthly average UTLS ozone column for collocated and
595 concurrent observations of AIRS, MLS, and ozonesonde during 2011 - 2017. The UTLS region
596 extends between 400 hPa to 70 hPa (Bian et al., 2007) for ozonesonde and AIRS, while for MLS,
597 the region between 261 hPa to 70 hPa is utilized. The recommended pressure levels for MLS v4
598 ozone retrieval are above 261 hPa (Livesey et al., 2013; Schwartz et al., 2015). In contrast to TCO,
599 higher ozone in UTLS is seen during the winter and spring (~ 45 DU) when there are recurring
600 downward transport events, while a clear drop of the column during the summer-monsoon shows
601 the convective transport of cleaner oceanic air to the higher altitudes. All the collocated
602 observations are able to capture the monthly variation effectively. However, there is a substantial
603 overestimation by more than 3 DU (Table S5) for all the months in AIRS measurements and MLS
604 mostly underestimate it, except during winter due to smaller integrated columns. Furthermore, the

larger whiskers of the box plot during winter and spring show the larger variations of the ozone in the UTLS region. Though there were notable overestimations compared to ozonesonde, still UTLS monthly variations are captured well by AIRS with a correlation of up to 75% (Table S4). In addition, the correlation of ozonesonde and AIRS ozone at each pressure level in the UTLS region is 0.81, which further increases with ozonesonde (AK) (of about 0.94). The persistent biases in the satellite retrievals arises due to inadequate input parameters that can be improved by using more accurate initial parameters and surface emissivity (Dufour et al., 2012; Boynard et al., 2018).

3.5.3 Tropospheric Ozone Column

Figure 10c shows the variations in the monthly average tropospheric ozone column utilizing various collocated data sets during 2011 - 2017. The tropospheric ozone column is calculated by integrating ozone profiles from the surface to the tropopause. WMO-defined lapse rate calculation method is used to calculate tropopause height from balloon-borne and AIRS observations (Figure 3). Higher tropospheric ozone is observed during the spring and early summer (> 45 DU) when annual crop-residue burning (Figure S7) events occur over northern India, apart from downward transport from the stratosphere. A few cases of downward transport are discussed in the next section. The tropospheric ozone column drops rapidly during the summer-monsoon when pristine marine air reaches Nainital. A slight increase of column is also seen during the autumn, which is again influenced by post-monsoon crop residue burning practices (Figure S7) over northern India (Bhardwaj et al., 2016). The AIRS is able to capture the monthly variations very effectively; however, there are larger biases. The biases with ozonesonde are higher when the tropopause is taken from the balloon-borne observation, while with AIRS provided tropopause, the biases are lesser or mostly within the one sigma limit. The correlation between ozonesonde and AIRS, when

used AIRS tropopause, is very strong (0.72). Like AIRS, the OMI/MLS column is in good agreement and able to produce monthly variations; however, there are larger differences during winter and spring of more than 10 DU. The tropospheric ozone column from ozonesonde is different for balloon-borne LRT and AIRS tropopause, which could be due to the lower vertical resolution of AIRS. AIRS calculates tropopause with an uncertainty of 1-2 km (Divakarla et al., 2006). It can also be seen that on average a lower (about 28%) tropopause pressure (or higher altitude) is calculated by AIRS compare to ozonesonde measurements (Figure 3).

3.6 Case Studies of Biomass Burning and Downward Transport

Over northern India, extensive agriculture practices and forest fires influence ozone at the surface and higher altitudes (Kumar et al., 2011; Cristofanelli et al., 2014; Bhardwaj et al., 2016; Bhardwaj et al., 2018). Based on MODIS fire counts, the days in between 1 March to 15 April over northern India are classified as the low fire periods (LFP) as considered in previous studies over this region. The high fire period (HFP) is classified when the fire counts over the observational site are more than the median fire counts in the biomass burning period, typically from mid-April to May (Bhardwaj et al., 2016). A total of 32 soundings (mid-April to May) are classified as HFP and 33 soundings (March to mid-April) are classified as LFP. Figure 11 (left) shows the average ozone profiles up to 6 km from ozonesonde and AIRS observations during HFP and LFP. The ozonesonde data show enhancement in ozone by about 5 ppbv to about 11 ppbv during HFP as compared to LFP that is accounting for a 5 - 20% increase. It is important to mention that enhancement is greater in higher altitude regions that drop gradually above 400 hPa. The enhancement is slightly lower (10 - 15%) in the AIRS profile, where most of it is contributed by the a-priori profile (Figure S8).

Deep stratospheric intrusion or the downward transport (DT) of ozone-rich air from the stratosphere to the troposphere significantly influences ozone profiles over the subtropical regions (Collins, et al., 2003; Zhu, et al., 2006; Lal et al., 2014). Over the subtropical Himalayas, such ozone intrusions are observed during the winter and spring seasons (Zhu et al., 2006; Ojha et al., 2014). The DT events are classified based on the higher ozone in middle - upper troposphere seen from ozonesonde with relatively larger Ertel potential vorticity (EPV) and lower humidity in MERRA-2 reanalysis data. Based on this, 10 soundings (between January and mid-April) are classified as DT events for ozonesonde and AIRS. Figure 11 (right) shows ozone profiles from ozonesonde (AK) and AIRS observations for high ozone DT events as well as the average ozone profiles of corresponding months excluding the DT event. Though there are persistent positive biases in AIRS ozone profile compared to ozonesonde in the middle/upper troposphere, still both the observations have captured the influence of the downward transport on the ozone profile very effectively and show an increase in the ozone of 10 - 20% in altitude range 2 - 16 km. Ozonesonde based observations have shown about twofold increase in upper-middle tropospheric ozone due to downward ozone transport over this region (Ojha et al., 2014). Further, the first guess profile's contribution to AIRS retrieval during DTs is negligible (Figure S9) and shows the main contribution from the AIRS observations itself. So, despite the persistent biases in the AIRS and ozonesonde observations, AIRS is able to capture the influences of downward transport (DT) on ozone profile notably well.

3.7 Ozone Radiative Forcing

Radiative forcing is a valuable metric to estimate the radiative impacts of any anthropogenic or natural activity on the climate system (Ramaswamy et al., 2001). It measures the net radiation at the surface, tropopause, and the top of the atmosphere due to any atmospheric constituents. Here we discuss the ozone radiative forcing (RF) at the surface in the ultraviolet (UV) spectral range (Antón et al., 2014; Mateos et al., 2020) using the ozonesonde, OMI, and AIRS total column ozone (TCO) data. The RF is calculated based on Antón et al. (2014), relative to 1979 utilizing TOMS TOC data in 1979, monthly averaged solar zenith angles of site, clearness index based on Chakraborty et al., (2014) and Hawas et al., (1984), and respective monthly average TCO data of AIRS, OMI, and ozonesonde. Rather than quantifying the RF values here, our primary focus is to show how the discrepancies of satellite ozone data (mainly AIRS) can impact the calculation of RF values. Figure 12 shows the seasonal average ozone radiative forcing (RF) relative to 1979. The annual average ozone RF during 2011 - 2017 is 4.86, 4.04, and 2.96 mWm^{-2} for ozonesonde, OMI, and AIRS, respectively. The RF values for ozonesonde and OMI are comparable to Mateos et al. (2020) (4 mWm^{-2}) for the extratropical region. However, for AIRS, the RF value is lower by 45%. Further, the seasonal average ozone RF (2011-2017) is consistent between ozonesonde and OMI, while notable differences are seen in AIRS except during the winter season when differences are marginal (Figure 12). Also, it is noted (Table 3) that the higher total ozone bias during autumn (as high as 22 DU) contributes to higher RF differences in autumn (Figure 12).

4. Summary and Conclusions

This study has utilized 242 ECC (EN-SCI) ozone soundings (during 2011 - 2017) conducted over the Himalayan station (Nainital) to evaluate the AIRS version 6 ozone product and study the

performance during biomass burning events, ozone downward transport events and estimation of ozone radiative forcing. AIRS ozone retrieval is evaluated in terms of retrieval sensitivity, retrieval biases, retrieval errors, and ability to retrieve the natural variability of columnar ozone at different altitude regions. This study is the first of its kind in the Himalayan region. The AIRS averaging kernels information was applied to ozonesonde for a like-for-like comparison to overcome their sensitivity differences. The monthly profile evaluation shows ozone peak and ozone altitude dependency is captured well by AIRS retrieval with smaller but notable underestimation (5 - 20%) in the lower-middle troposphere and stratosphere, while overestimation in the UTLS region as high as 102%. We show a relatively higher sensitivity of AIRS ozone for the summer monsoon in the UTLS region, where the biases between AIRS and ozonesonde reduced from 92% to 19 % after applying AIRS averaging kernel information.

Furthermore, the weighted statistical error analysis of AIRS retrieved ozone profiles with ozonesonde shows higher positive biases (65%) and STD (25%) in the upper troposphere. While in the lower-middle troposphere and stratosphere, AIRS ozone was negatively biased of less than 20%. In addition, though the biases and errors are higher in the upper troposphere, there is a larger correlation of about 81%, demonstrating the reasonable capability of AIRS to retrieve upper tropospheric ozone variability with certain positive biases. Such biases in satellite retrieval can be eliminated by choosing better emissivity inputs or other retrieval parameters.

The histogram of differences between AIRS and ozonesonde (AK) demonstrated that AIRS mostly underestimated ozone (2.37 - 39.8 ppbv), while a notable overestimation with a mean bias of about 43 ppbv is seen in the upper troposphere. The AIRS ozone retrieval algorithm was further

719 evaluated using the radiance of IASI and CrIS sensors; these sensors provided similar error
720 statistics as seen for AIRS, with higher positive biases in the UTLS region.

721 The AIRS-derived columnar ozone amounts (i.e., total, UTLS, and tropospheric ozone) are also
722 evaluated to see whether the ozone variability at different altitude regions is being retrieved
723 correctly. The UTLS and tropospheric ozone monthly variations are captured well by AIRS with
724 persistent positive biases. However, the total ozone column shows bimodal monthly variations,
725 which was not evident in the ozonesonde and OMI total ozone observations. Further, we found a
726 higher total ozone column in AIRS during autumn, which is mostly coming from the stratospheric
727 region above 50 hPa. Furthermore, the capabilities of AIRS ozone retrieval to capture various
728 biomass burning and downward transport events have also been studied using fire counts and EPV
729 tracers. AIRS captures reasonable enhancements in ozone profiles (5 - 20%) after such events with
730 notable contributions of the a-priori, particularly in biomass-burning events.Unlike the well-mixed
731 greenhouse gases, the ozone radiative forcing (RF) remains uncertain due to inadequate budget
732 estimates and complex chemical processes. Stevenson et al. (2013) have shown that a few percent
733 uncertainties in ozone concentrations can produce a spread of ~17% in ozone RF estimations. The
734 total ozone discrepancies of AIRS lead to show lower RF (by about 45%) compared to ozonesonde
735 and OMI and higher uncertainty in this Himalayan region. Here, the role of in-situ observations
736 from ozone soundings is shown to be important in improving the satellite-retrieved ozone over the
737 Himalayan region by assessing and providing insights upon its errors and biases. This information
738 could be applied to the ozone retrieval from other satellite data sets, having long-term coverage.
739 This will help better understand regional ozone and radiation budgets over this Himalayan region
740 and offer an opportunity to understand possible differences between satellites and truth
741 observations.

Acknowledgments

We are grateful to Director ARIES and ISRO-ATCTM project for supporting this work. Help from Deepak and Nitin in balloon launches and coordination with the air traffic control is highly acknowledged. The National Center for Atmospheric Research is sponsored by the National Science Foundation. SL is grateful to INSA, New Delhi for the position and Director PRL, Ahmedabad for the support. We highly acknowledge NOAA and NASA-EARTHDATA online data portals for providing IASI, AIRS, and CrIS label2 data. We thank the NASA Goddard Space Flight Center Ozone Processing Team for providing the OMI/MLS tropospheric ozone, OMI total ozone column and JPL for MLS ozone profile. We would also like to acknowledge the use of the MODIS fire data through FIRMS archive download. Use of map from Google earth is also acknowledged. We thank the reviewers for their constructive comments and valuable suggestions.

Data availability: Satellite data are available in the respective web portal. Ozonesonde data could be made available on a reasonable request by writing to the corresponding author.

References

Antón, M., D. Mateos, R. Román, A. Valenzuela, L. Alados-Arboledas, and F. J. Olmo.: A method to determine the ozone radiative forcing in the ultra-violet range from experimental data, J. Geophys. Res. Atmos., 119, 1860–1873, doi:10.1002/2013JD020444, 2014.

Aghedo, A.M., Bowman, K.W., Worden, H.M., Kulawik, S.S., Shindell, D.T., Lamarque, J.F., Faluvegi, G., Parrington, M., Jones, D.B.A. and Rast, S.: The vertical distribution of ozone

764 instantaneous radiative forcing from satellite and chemistry climate models. Journal of
765 Geophysical Research: Atmospheres, 116(D1), 2011.
766
767 Bai, W., Wu, C., Li, J. and Wang, W.: Impact of terrain altitude and cloud height on ozone remote
768 sensing from satellite, Journal of Atmospheric and Oceanic Technology, 31(4), pp.903-912, 2014.
769
770 Barre, J., Peuch, V.H., Attié, J.L., Amraoui, L.E., Lahoz, W.A., Josse, B., Claeyman, M. and
771 Nedelec, P.: Stratosphere-troposphere ozone exchange from high resolution MLS ozone analyses,
772 Atmos. Chem. Phys., 12(14), pp.6129-6144, 2012.
773
774 Bhardwaj, P., Naja, M., Kumar, R. and Chandola, H.C.: Seasonal, interannual, and long-term
775 variabilities in biomass burning activity over South Asia, Environmental Science and Pollution
776 Research, 23(5), pp.4397-4410, 2016.
777
778 Bhardwaj, P., Naja, M., Rupakheti, M., Lupascu, A., Mues, A., Panday, A. K., Kumar, R., Mahata,
779 K. S., Lal, S., Chandola, H. C., and Lawrence, M. G.: Variations in surface ozone and carbon
780 monoxide in the Kathmandu Valley and surrounding broader regions during SusKat-ABC field
781 campaign: role of local and regional sources, Atmos. Chem. Phys., 18, 11949–11971,
782 https://doi.org/10.5194/acp-18-11949-2018, 2018.
783
784 Bhartia, P.K., McPeters, R.D., Mateer, C.L., Flynn, L.E. and Wellemeyer, C.: Algorithm for the
785 estimation of vertical ozone profiles from the backscattered ultraviolet technique, J. Geophys. Res.
786 Atmos., 101(D13), pp.18793-18806, 1996.
787

788 Bian, J., Gettelman, A., Chen, H. and Pan, L.L.: Validation of satellite ozone profile retrievals
789 using Beijing ozonesonde data, J. Geophys. Res. Atmos., 112(D6), 2007.
790
791 Boynard, A., Hurtmans, D., Koukouli, M.E., Goutail, F., Bureau, J., Safieddine, S., Lerot, C.,
792 Hadji-Lazaro, J., Wespes, C., Pommereau, J.P. and Pazmino, A.: Seven years of IASI ozone
793 retrievals from FORLI: validation with independent total column and vertical profile
794 measurements, Atmos. Meas. Tech., 9(9), pp.4327-4353, 2016.
795
796 Boynard, A., Hurtmans, D., Garane, K., Goutail, F., Hadji-Lazaro, J., Koukouli, M. E., Wespes,
797 C., Vigouroux, C., Keppens, A., Pommereau, J.-P., Pazmino, A., Balis, D., Loyola, D., Valks, P.,
798 Sussmann, R., Smale, D., Coheur, P.-F., and Clerbaux, C.: Validation of the IASI
799 FORLI/EUMETSAT ozone products using satellite (GOME-2), ground-based (Brewer–Dobson,
800 SAOZ, FTIR) and ozonesonde measurements, Atmos. Meas. Tech., 11, 5125–5152,
801 https://doi.org/10.5194/amt-11-5125-2018, 2018.
802
803 Brunamonti S. et al.,: Balloon-borne measurements of temperature, water vapor, ozone and aerosol
804 backscatter on the southern slopes of the Himalayas during StratoClim 2016–2017, Atmos. Chem. Phys.,
805 18, 15937–15957, https://doi.org/10.5194/acp-18-15937-2018, 2018.
806
807 Chakraborty, S., Sadhu, P.K. and Nitai, P.A.L.: New location selection criterions for solar PV
808 power plant. International Journal of Renewable Energy Research, 4(4), pp.1020-1030, 2014.
809
810 Clerbaux, C., Hadji-Lazaro, J., Turquety, S., George, M., Coheur, P.F., Hurtmans, D., Wespes, C.,
811 Herbin, H., Blumstein, D., Tourniers, B. and Phulpin, T.: The IASI/MetOp1 Mission: First

observations and highlights of its potential contribution to GMES2, Space Research Today, 168, pp.19-24, 2007.

Coheur, P.F., Barret, B., Turquety, S., Hurtmans, D., Hadji-Lazaro, J. and Clerbaux, C.: Retrieval and characterization of ozone vertical profiles from a thermal infrared nadir sounder, J. Geophys. Res. Atmos., 110(D24), 2005.

Collins, W. J., R. G. Derwent, B. Garnier, C. E. Johnson, M. G. Sanderson, and D. S. Stevenson.: Effect of stratosphere-troposphere exchange on the future tropospheric ozone trend, J. Geophys. Res., 108(D12), 8528, doi:10.1029/2002JD002617, 2003.

Cristofanelli, P., Putero, D., Adhikary, B., Landi, T.C., Marinoni, A., Duchi, R., Calzolari, F., Laj, P., Stocchi, P., Verza, G. and Vuillermoz, E.: Transport of short-lived climate forcers/pollutants (SLCF/P) to the Himalayas during the South Asian summer monsoon onset, Environmental Research Letters, 9(8), p.084005, 2014.

Divakarla, M., Barnet, C., Goldberg, M., Maddy, E., Wolf, W., Flynn, L., Xiong, X., Wei, J., Zhou, L. and Liu, X.: Validation of Atmospheric Infrared Sounder (AIRS) temperature, water vapor, and ozone retrievals with matched radiosonde and ozonesonde measurements and forecasts, In Multispectral, Hyperspectral, and Ultraspectral Remote Sensing Technology, Techniques, and Applications, International Society for Optics and Photonics, Vol. 6405, p. 640503, 2006.

834 Divakarla, M., Barnet, C., Goldberg, M., Maddy, E., Irion, F., Newchurch, M., Liu, X., Wolf, W.,
835 Flynn, L., Labow, G. and Xiong, X.: Evaluation of Atmospheric Infrared Sounder ozone profiles
836 and total ozone retrievals with matched ozonesonde measurements, ECMWF ozone data, and
837 Ozone Monitoring Instrument retrievals, J. Geophys. Res. Atmos., 113(D15), 2008.
838
839 Dufour, G., Eremenko, M., Griesfeller, A., Barret, B., LeFlochmoën, E., Clerbaux, C., Hadji-
840 Lazaro, J., Coheur, P.F. and Hurtmans, D.: Validation of three different scientific ozone products
841 retrieved from IASI spectra using ozonesondes, Atmos. Meas. Tech., 5(3), pp.611-630, 2012.
842
843 Ebi, K.L. and McGregor, G., Climate change, tropospheric ozone and particulate matter, and health
844 impacts, Environmental health perspectives, 116(11), pp.1449-1455, 2008.
845
846 Fadnavis, S., Dhomse, S., Ghude, S., Iyer, U., Buchunde, P., Sonbawne, S. and Raj, P.E.: Ozone
847 trends in the vertical structure of Upper Troposphere and Lower stratosphere over the Indian
848 monsoon region, International Journal of Environmental Science and Technology, 11(2), pp.529-
849 542, 2014.
850
851 Finlayson-Pitts, B.J. and Pitts, J.N.: Tropospheric air pollution: ozone, airborne toxics, polycyclic
852 aromatic hydrocarbons, and particles, Science, 276(5315), pp.1045-1051, 1997.
853
854 Fishbein, E., Farmer, C.B., Granger, S.L., Gregorich, D.T., Gunson, M.R., Hannon, S.E.,
855 Hofstadter, M.D., Lee, S.Y., Leroy, S.S. and Strow, L.L.: Formulation and validation of simulated

856 data for the Atmospheric Infrared Sounder (AIRS), IEEE Transactions on Geoscience and Remote
857 Sensing, 41(2), pp.314-329, 2003.
858
859 Fishman, J., Ramanathan, V., Crutzen, P.J. and Liu, S.C.: Tropospheric ozone and climate, Nature,
860 282(5741), pp.818-820, 1979.
861
862 Fishman, J., Minnis, P. and Reichle Jr, H.G.: Use of satellite data to study tropospheric ozone in
863 the tropics, J. Geophys. Res. Atmos., 91(D13), pp.14451-14465, 1986.
864
865 Fishman, J. and Larsen, J.C.: Distribution of total ozone and stratospheric ozone in the tropics:
866 Implications for the distribution of tropospheric ozone, J. Geophys. Res. Atmos., 92(D6), pp.6627-
867 6634, 1987.
868
869 Foret, G., Eremenko, M., Cuesta, J., Sellitto, P., Barré, J., Gaubert, B., Coman, A., Dufour, G.,
870 Liu, X., Joly, M. and Doche, C.: Ozone pollution: What can we see from space? A case study, J.
871 Geophys. Res. Atmos., 119(13), pp.8476-8499, 2014.
872
873 Forster, P.M., Bodeker, G., Schofield, R., Solomon, S. and Thompson, D.: Effects of ozone cooling
874 in the tropical lower stratosphere and upper troposphere, Geophysical Research Letters, 34(23),
875 2007.
876
877 Fry, M.M., Naik, V., West, J.J., Schwarzkopf, M.D., Fiore, A.M., Collins, W.J., Dentener, F.J.,
878 Shindell, D.T., Atherton, C., Bergmann, D. and Duncan, B.N.: The influence of ozone precursor

879 emissions from four world regions on tropospheric composition and radiative climate forcing.
880 Journal of Geophysical Research: Atmospheres, 117(D7), 2012.
881
882 Gauss, M., Myhre, G., Pitari, G., Prather, M.J., Isaksen, I.S.A., Berntsen, T.K., Brasseur, G.P.,
883 Dentener, F.J., Derwent, R.G., Hauglustaine, D.A. and Horowitz, L.W.: Radiative forcing in the
884 21st century due to ozone changes in the troposphere and the lower stratosphere, J. Geophys. Res.
885 Atmos., 108(D9), 2003.
886
887 Hauglustaine, D.A. and Brasseur, G.P.: Evolution of tropospheric ozone under anthropogenic
888 activities and associated radiative forcing of climate, J. Geophys. Res. Atmos., 106(D23),
889 pp.32337-32360, 2001.
890
891 Hawas, M.M. and Muneer, T.; Study of diffuse and global radiation characteristics in
892 India. Energy Conversion and Management, 24(2), pp.143-149, 1984.
893
894 Hudson, R.D. and Thompson, A.M.: Tropical tropospheric ozone from total ozone mapping
895 spectrometer by a modified residual method, J. Geophys. Res. Atmos., 103(D17), pp.22129-
896 22145, 1998.
897
898 Hegglin, M. I., Fahey, D. W., McFarland, M., Montzka, S. A., and Nash, E. R.: Twenty questions
899 and answers about the ozone layer: 2014 update, Scientific Assessment of Ozone Depletion: 2014,
900 84 pp., World Meteorological Organization, Geneva, Switzerland, ISBN 978-9966-076-02-1,
901 2015.

Irion, F.W., Kahn, B.H., Schreier, M.M., Fetzer, E.J., Fishbein, E., Fu, D., Kalmus, P., Wilson, R.C., Wong, S. and Yue, Q.: Single-footprint retrievals of temperature, water vapor and cloud properties from AIRS. Atmospheric Measurement Techniques, 11(2), pp.971-995, 2018.

Kim, J.H. and Newchurch, M.J.: Climatology and trends of tropospheric ozone over the eastern Pacific Ocean: The influences of biomass burning and tropospheric dynamics, Geophysical research letters, 23(25), pp.3723-3726, 1996.

Komhyr, W.D., Barnes, R.A., Brothers, G.B., Lathrop, J.A. and Opperman, D.P.: Electrochemical concentration cell ozonesonde performance evaluation during STOIC 1989, J. Geophys. Res. Atmos., 100(D5), pp.9231-9244, 1995.

Komhyr, W.D.: Nonreactive gas sampling pump. Review of Scientific Instruments, 38(7), pp.981-983, 1967.

Kumar, R., Naja, M., Satheesh, S.K., Ojha, N., Joshi, H., Sarangi, T., Pant, P., Dumka, U.C., Hegde, P. and Venkataramani, S.: Influences of the springtime northern Indian biomass burning over the central Himalayas. Journal of Geophysical Research: Atmospheres, 116(D19), 2011.

Kumar, R., Naja, M., Pfister, G.G., Barth, M.C. and Brasseur, G.P.: Simulations over South Asia using the Weather Research and Forecasting model with Chemistry (WRF-Chem): set-up and meteorological evaluation, Geoscientific Model Development, 5(2), pp.321-343, 2012a.

925

926 Kumar, R., Naja, M., Pfister, G.G., Barth, M.C., Wiedinmyer, C. and Brasseur, G.P.: Simulations
927 over South Asia using the Weather Research and Forecasting model with Chemistry (WRF-
928 Chem): chemistry evaluation and initial results, Geoscientific Model Development, 5(3), pp.619-
929 648, 2012b.

930

931 Lacis, A.A., Wuebbles, D.J. and Logan, J.A.: Radiative forcing of climate by changes in the
932 vertical distribution of ozone, J. Geophys. Res. Atmos., 95(D7), pp.9971-9981, 1990.

933

934 Lal S., S. Venkataramani, S. Srivastava, S. Gupta, M. Naja, T. Sarangi, X. Liu.: Transport effects
935 on the vertical distribution of tropospheric ozone over the tropical marine regions surrounding
936 India, J. Geophys. Res.,118, 1513-1524, doi:10.1002/jgrd.50180, 2013.

937

938 Lal S., S. Venkataramani, N. Chandra, O. R. Cooper, J. Brioude, and M. Naja, Transport effects
939 on the vertical distribution of tropospheric ozone over western India, J. Geophys. Res. Atmos.,
940 119, doi:10.1002/2014JD021854, 2014.

941

942 Lal, S., Venkataramani, S., Naja, M., Kuniyal, J.C., Mandal, T.K., Bhuyan, P.K., Kumari, K.M.,
943 Tripathi, S.N., Sarkar, U., Das, T. and Swamy, Y.V.: Loss of crop yields in India due to surface
944 ozone: An estimation based on a network of observations, Environmental Science and Pollution
945 Research, 24(26), pp.20972-20981, 2017.

946

947 Lawrence, M.G. and Lelieveld, J.: Atmospheric pollutant outflow from southern Asia: a review,
948 Atmospheric Chemistry and Physics, 10(22), pp.11017-11096, 2010.
949
950 Lelieveld, J., Haines, A. and Pozzer, A.: Age-dependent health risk from ambient air pollution: a
951 modelling and data analysis of childhood mortality in middle-income and low-income countries,
952 The lancet Planetary health, 2(7), pp.e292-e300, 2018.
953
954 Livesey, N.J., Logan, J.A., Santee, M.L., Waters, J.W., Doherty, R.M., Read, W.G., Froidevaux,
955 L. and Jiang, J.H.; Interrelated variations of O 3, CO and deep convection in the
956 tropical/subtropical upper troposphere observed by the Aura Microwave Limb Sounder (MLS)
957 during 2004–2011. Atmospheric Chemistry and Physics, 13(2), pp.579-598, 2013.
958
959 Logan, J.A.: Tropospheric ozone: Seasonal behavior, trends, and anthropogenic influence, J.
960 Geophys. Res. Atmos., 90(D6), pp.10463-10482, 1985.
961
962 Lu, X., Zhang, L., Liu, X., Gao, M., Zhao, Y. and Shao, J., 2018. Lower tropospheric ozone over
963 India and its linkage to the South Asian monsoon. Atmospheric Chemistry and Physics, 18(5),
964 pp.3101-3118.
965
966 Maddy, E.S. and Barnet, C.D.: Vertical resolution estimates in version 5 of AIRS operational
967 retrievals, IEEE Transactions on Geoscience and Remote Sensing, 46(8), pp.2375-2384, 2008.
968

969 Mateos, D. and Antón, M.: Worldwide Evaluation of Ozone Radiative Forcing in the UV-B Range
970 between 1979 and 2014. Remote Sensing, 12(3), p.436, 2020.
971
972 McPeters, R.D., Miles, T., Flynn, L.E., Wellemeyer, C.G. and Zawodny, J.M.: Comparison of
973 SBUV and SAGE II ozone profiles: Implications for ozone trends, J. Geophys. Res. Atmos.,
974 99(D10), pp.20513-20524, 1994.
975
976
977 McPeters, R.D., Labow, G.J. and Logan, J.A.: Ozone climatological profiles for satellite retrieval
978 algorithms, J. Geophys. Res. Atmos., 112(D5), 2007.
979
980 McPeters, R.D. and Labow, G.J.,: Climatology 2011: An MLS and sonde derived ozone
981 climatology for satellite retrieval algorithms. Journal of Geophysical Research:
982 Atmospheres, 117(D10), 2012.
983 Monahan, K.P., Pan, L.L., McDonald, A.J., Bodeker, G.E., Wei, J., George, S.E., Barnet, C.D. and
984 Maddy, E.: Validation of AIRS v4 ozone profiles in the UTLS using ozonesondes from Lauder,
985 NZ and Boulder, USA, J. Geophys. Res. Atmos., 112(D17), 2007.
986
987 Monks, P.S., Archibald, A.T., Colette, A., Cooper, O., Coyle, M., Derwent, R., Fowler, D.,
988 Granier, C., Law, K.S., Mills, G.E. and Stevenson, D.S.: Tropospheric ozone and its precursors
989 from the urban to the global scale from air quality to short-lived climate forcer. Atmospheric
990 Chemistry and Physics, 15(15), pp.8889-8973, 2015.
991

992 Munro, R., Siddans, R., Reburn, W.J. and Kerridge, B. J.: Direct measurement of tropospheric
993 ozone distributions from space, Nature, 392(6672), pp.168-171, 1998.
994
995 Myhre, G., Aas, W., Cherian, R., Collins, W., Faluvegi, G., Flanner, M., Forster, P., Hodnebrog,
996 Ø., Klimont, Z., Lund, M.T. and Mülmenstädt, J.: Multi-model simulations of aerosol and ozone
997 radiative forcing due to anthropogenic emission changes during the period 1990–2015.
998 Atmospheric Chemistry and Physics, 17(4), pp.2709-2720, 2017.
999
1000 Naja, M., C Mallik, T. Sarangi, V Sheel, S. Lal, SO2 measurements at a high altitude site in the
1001 central Himalayas: Role of regional transport, Atmospheric Environment,
1002 doi:10.1016/j.atmosenv.2014.08.031, 2014.
1003
1004 Naja M., Piyush Bhardwaj, N. Singh, Phani Kumar, R. Kumar, N. Ojha, Ram Sagar, S. K.
1005 Satheesh, K. Krishna Moorthy and V. R. Kotamarthi: High-frequency vertical profiling of
1006 meteorological parameters using AMF1 facility during RAWEX–GVAX at ARIES, Nainital,
1007 Current Science, vol 111, issue 1, 2016.
1008
1009 Nalli, N.R., Barnet, C.D., Reale, A., Tobin, D., Gambacorta, A., Maddy, E.S., Joseph, E., Sun, B.,
1010 Borg, L., Mollner, A.K. and Morris, V.R.: Validation of satellite sounder environmental data
1011 records: Application to the Cross-track Infrared Microwave Sounder Suite, J. Geophys. Res.
1012 Atmos., 118(24), pp.13-628, 2013.
1013
1014 Nalli, N.R., Gambacorta, A., Liu, Q., Tan, C., Iturbide-Sanchez, F., Barnet, C.D., Joseph, E.,
1015 Morris, V.R., Oyola, M. and Smith, J.W.: Validation of Atmospheric Profile Retrievals from the

SNPP NOAA-Unique Combined Atmospheric Processing System. Part 2: Ozone, IEEE Transactions on Geoscience and Remote Sensing, 56(1), pp.598-607, 2017.

Nassar, R., Logan, J.A., Worden, H.M., Megretskaia, I.A., Bowman, K.W., Osterman, G.B., Thompson, A.M., Tarasick, D.W., Austin, S., Claude, H. and Dubey, M.K. Validation of Tropospheric Emission Spectrometer (TES) nadir ozone profiles using ozonesonde measurements. Journal of Geophysical Research: Atmospheres, 113(D15), 2008.

Ojha, N., Naja, M., Sarangi, T., Kumar, R., Bhardwaj, P., Lal, S., Venkataramani, S., Sagar, R., Kumar, A. and Chandola, H.C.: On the processes influencing the vertical distribution of ozone over the central Himalayas: Analysis of yearlong ozonesonde observations, Atmospheric Environment, 88, pp.201-211, 2014.

Pagano, T.S., Aumann, H.H., Hagan, D.E. and Overoye, K.: Prelaunch and in-flight radiometric calibration of the Atmospheric Infrared Sounder (AIRS), IEEE transactions on geoscience and remote sensing, 41(2), pp.265-273, 2003.

Pierce, R.B., Al-Saadi, J., Kittaka, C., Schaack, T., Lenzen, A., Bowman, K., Szykman, J., Soja, A., Ryerson, T., Thompson, A.M. and Bhartia, P.: Impacts of background ozone production on Houston and Dallas, Texas, air quality during the Second Texas Air Quality Study field mission, J. Geophys. Res. Atmos., 114(D7), 2009.

Pittman, J.V., Pan, L.L., Wei, J.C., Irion, F.W., Liu, X., Maddy, E.S., Barnet, C.D., Chance, K. and Gao, R.S.: Evaluation of AIRS, IASI, and OMI ozone profile retrievals in the extratropical tropopause region using in situ aircraft measurements, J. Geophys. Res. Atmos., 114(D24), 2009.

Ramaswamy, V., Boucher, O., Haigh, J., Hauglustaine, D., Haywood, J., Myhre, G., Nakajima, T., Shi, G.Y. and Solomon, S.: Radiative forcing of climate change. Climate change 2001: the scientific basis. Contribution of working group I to the third assessment report of the intergovernmental panel on climate change. DJ Griggs, M Noguer, PJ van der Linden, X Dai, K Maskell and CA Johnson (Cambridge: Cambridge University Press) pp, 350, p.416, 2001.

Rawat, P., Naja, M., Thapliyal, P.K., Srivastava, S., Bhardwaj, P., Kumar, R., Bhatacharjee, S., Venkatramani, S., Tiwari, S.N. and Lal, S.: Assessment of vertical ozone profiles from INSAT-3D sounder over the Central Himalaya. Current Science, 119(7), p.1113, 2020.

Rawat, P. and Naja, M.: Remote sensing study of ozone, NO2, and CO: some contrary effects of SARS-CoV-2 lockdown over India. Environ Sci Pollut Res, https://doi.org/10.1007/s11356-021-17441-2, 2021.

Rodgers, C.D., 1976. Retrieval of atmospheric temperature and composition from remote measurements of thermal radiation. Reviews of Geophysics, 14(4), pp.609-624.

Rodgers, C.D., 1990. Characterization and error analysis of profiles retrieved from remote sounding measurements. Journal of Geophysical Research: Atmospheres, 95(D5), pp.5587-5595.

Rodgers, C.D. and Connor, B.J., 2003. Intercomparison of remote sounding instruments. Journal of Geophysical Research: Atmospheres, 108(D3).

Sarangi T., M. Naja, N. Ojha, R. Kumar, S. Lal, S. Venkataramani, A. Kumar, R. Sagar and H. C. Chandola: First simultaneous measurements of ozone, CO and NO_y at a high altitude regional representative site in the central Himalayas, J. Geophys. Res., 119, doi:10.1002/2013JD020631, 2014.

Schwartz, M., Froidevaux, L., Livesey, N. and Read, W.: MLS/Aura Level 2 Ozone (O3) Mixing Ratio V004, Greenbelt, MD, USA, Goddard Earth Sciences Data and Information Services Center (GES DISC), 10.5067/Aura/MLS/DATA2017, 2015.

Shindell, D., Kuylenstierna, J.C., Vignati, E., van Dingenen, R., Amann, M., Klimont, Z., Anenberg, S.C., Muller, N., Janssens-Maenhout, G., Raes, F. and Schwartz, J.: Simultaneously mitigating near-term climate change and improving human health and food security, Science, 335(6065), pp.183-189, 2012.

Smit, H.G., Straeter, W., Johnson, B.J., Oltmans, S.J., Davies, J., Tarasick, D.W., Hoegger, B., Stubi, R., Schmidlin, F.J., Northam, T. and Thompson, A.M.: Assessment of the performance of ECC-ozonesondes under quasi-flight conditions in the environmental simulation chamber: Insights from the Juelich Ozone Sonde Intercomparison Experiment (JOSIE), Journal of Geophysical Research: Atmospheres, 112(D19), 2007.

Smit, H. G. J., Thompson, A. M., & ASOPOS Panel. (2020). ASOPOS 2.0: Assessment of Standard Operating Procedures for Ozone Sondes, WMO/GAW Report.

Srivastava S., Manish Naja, V. Thouret: Influences of regional pollution and long range transport over Hyderabad using ozone data from MOZAIC, Atmospheric Environment, 117, pp.135-146, 2015.

Stauffer, R.M., Thompson, A.M., Kollonige, D.E., Tarasick, D.W., Van Malderen, R., Smit, H.G., Vömel, H., Morris, G.A., Johnson, B.J., Cullis, P.D. and Stübi, R.: An examination of the recent stability of ozonesonde global network data. Earth and Space Science, 9(10), p.e2022EA002459, 2022.

Stevenson, D.S., Young, P.J., Naik, V., Lamarque, J.F., Shindell, D.T., Voulgarakis, A., Skeie, R.B., Dalsoren, S.B., Myhre, G., Berntsen, T.K. and Folberth, G.A.: Tropospheric ozone changes, radiative forcing and attribution to emissions in the Atmospheric Chemistry and Climate Model Intercomparison Project (ACCMIP), Atmos. Chem. Phys., 13(6), pp.3063-3085, 2013.

Susskind, J., Barnet, C.D. and Blaisdell, J.M.: Retrieval of atmospheric and surface parameters from AIRS/AMSU/HSB data in the presence of clouds, IEEE Transactions on Geoscience and Remote Sensing, 41(2), pp.390-409, 2003.

Susskind, J., Barnet, C., Blaisdell, J., Iredell, L., Keita, F., Kouvaris, L., Molnar, G. and Chahine, M.: Accuracy of geophysical parameters derived from Atmospheric Infrared Sounder/Advanced

Microwave Sounding Unit as a function of fractional cloud cover, J. Geophys. Res. Atmos., 111(D9), 2006.

Tarasick, D., Galbally, I.E., Cooper, O.R., Schultz, M.G., Ancellet, G., Leblanc, T., Wallington, T.J., Ziemke, J., Liu, X., Steinbacher, M. and Staehelin, J.: Tropospheric Ozone Assessment Report: Tropospheric ozone from 1877 to 2016, observed levels, trends and uncertainties. Elementa: Science of the Anthropocene, 7, 2019.

Thornhill, G.D., Collins, W.J., Kramer, R.J., Olivié, D., Skeie, R.B., O'Connor, F.M., Abraham, N.L., Checa-Garcia, R., Bauer, S.E., Deushi, M. and Emmons, L.K.: Effective radiative forcing from emissions of reactive gases and aerosols–a multi-model comparison. Atmospheric Chemistry and Physics, 21(2), pp.853-874, 2021.

Veefkind, J.P., de Haan, J.F., Brinksma, E.J., Kroon, M. and Levelt, P.F.: Total ozone from the Ozone Monitoring Instrument (OMI) using the DOAS technique, IEEE transactions on geoscience and remote sensing, 44(5), pp.1239-1244, 2006.

Verstraeten, W. W., Boersma, K. F., Zörner, J., Allaart, M. A. F., Bowman, K. W., and Worden, J. R.: Validation of six years of TES tropospheric ozone retrievals with ozonesonde measurements: implications for spatial patterns and temporal stability in the bias, Atmos. Meas. Tech., 6, 1413–1423, https://doi.org/10.5194/amt-6-1413-2013, 2013.

Wang, W.C., Zhuang, Y.C. and Bojkov, R.D.: Climate implications of observed changes in ozone vertical distributions at middle and high latitudes of the Northern Hemisphere, Geophysical research letters, 20(15), pp.1567-1570, 1993.

Wang, B., R. Wu, K.-M. Lau: Interannual variability of Asian summer monsoon: Contrast between the Indian and western North Pacific-East Asian monsoons. J. Climate, 14, 4073-4090, 2001.

Wang, H.R., Damadeo, R., Flittner, D., Kramarova, N., Taha, G., Davis, S., Thompson, A.M., Strahan, S., Wang, Y., Froidevaux, L. and Degenstein, D.: Validation of SAGE III/ISS Solar Occultation Ozone Products With Correlative Satellite and Ground-Based Measurements. Journal of Geophysical Research: Atmospheres, 125(11), p.e2020JD032430, 2020.

Wang, W., Cheng, T., van der A, R.J., de Laat, J. and Williams, J.E.: Verification of the Atmospheric Infrared Sounder (AIRS) and the Microwave Limb Sounder (MLS) ozone algorithms based on retrieved daytime and night-time ozone, Atmos. Meas. Tech., 14(2), pp.1673-1687, 2021.

Zhang, L., Jacob, D.J., Liu, X., Logan, J.A., Chance, K., Eldering, A. and Bojkov, B.R.: Intercomparison methods for satellite measurements of atmospheric composition: application to tropospheric ozone from TES and OMI. Atmospheric Chemistry and Physics, 10(10), pp.4725-4739, 2010.

Zhu, T., W. Lin,Y. Song, X. Cai, H. Zou, L. Kang, L. Zhou, and H. Akimoto: Downward transport of ozone-rich air near Mt. Everest, Geophys. Res. Lett., 33, L23809,doi:10.1029/2006GL027726, 2006.

Ziemke, J.R., Chandra, S. and Bhartia, P. K.: Two new methods for deriving tropospheric column ozone from TOMS measurements: Assimilated UARS MLS/HALOE and convective-cloud differential techniques, J. Geophys. Res. Atmos., 103(D17), pp.22115-22127, 1998.

Ziemke, J.R., Chandra, S., Duncan, B.N., Froidevaux, L., Bhartia, P.K., Levelt, P.F. and Waters, J.W.: Tropospheric ozone determined from Aura OMI and MLS: Evaluation of measurements and comparison with the Global Modeling Initiative's Chemical Transport Model, J. Geophys. Res. Atmos., 111(D19), 2006.

Zhang, R., Wang, H., Qian, Y., Rasch, P.J., Easter, R.C., Ma, P.L., Singh, B., Huang, J. and Fu, Q.: Quantifying sources, transport, deposition, and radiative forcing of black carbon over the Himalayas and Tibetan Plateau. Atmospheric Chemistry and Physics, 15(11), pp.6205-6223, 2015.

Table 1. The mean values and corresponding standard errors of ozone mixing ratio (ppbv) from ozonesonde, ozonesonde (AK) and AIRS over Nainital at six pressure levels and during winter, spring, summer-monsoon, autumn are given. The number of ozonesonde flights during four seasons are mentioned in the bracket.

Pressure levels		706 (hPa)	496 (hPa)	300 (hPa)	103 (hPa)	29 (hPa)	14.4 (hPa)
Winter (61)	ozonesonde	55.1±0.9	54.4±0.7	69.5±2.8	238.8±15.0	4569.3±67.8	7620.6±140.1
	ozonesonde (AK)	48.6±0.4	55.9±0.6	70.4±1.8	187.3±3.6	5249.1±78.8	8214.9±105.7
	AIRS	46.5±0.3	52.2±0.6	68.7±1.2	354.4±8.4	4428.2±55.8	6616.4±56.0
Spring (72)	ozonesonde	71.6±1.8	70.2±1.5	81.5±2.8	223.9±12.7	4747.0±42.6	8242.3±101.6
	ozonesonde (AK)	58.7±0.7	69.1±1.1	80.3±1.4	221.8±3.6	5137.8±63.4	8784.4±96.6
	AIRS	55.3±0.4	60.7±0.7	78.6±1.0	389.2±6.0	4687.4±38.2	7852.4±97.0
Summer-monsoon (55)	ozonesonde	53.0±2.7	65.1±2.7	82.1±2.5	138.6±3.4	4642.9±26.4	8493.6±91.1
	ozonesonde (AK)	44.1±1.2	62.3±1.7	68.7±1.7	224.3±3.4	5271.3±44.6	9233.8±72.4
	AIRS	48.8±0.5	57.5±0.5	63.6±0.6	267.4±5.5	4710.0±48.2	8333.1±82.5
Autumn (54)	ozonesonde	53.0±1.1	63.8±1.6	72.7±1.6	144.6±6.2	4439.3±28.2	8613.7±77.5
	ozonesonde (AK)	50.4±0.5	61.0±0.8	64.1±0.9	169.0±2.0	5086.3±38.7	9035.8±80.7
	AIRS	46.0±0.3	51.3±0.4	56.9±30.5	241.8±3.6	4635.4±43.9	7984.9±97.6

Table 2. Coefficient of determination (r^2) of three IR satellite sensors (AIRS, IASI and CrIS) ozone retrieval in five broad layers with respect to ozonesonde observations.

	Coefficient of determination (r^2)		
	AIRS	IASI	CrIS
600 - 800 hPa	0.52	0.34	0.09
300 - 600 hPa	0.44	0.31	0.22
100 - 300 hPa	0.45	0.44	0.45
50-100 hPa	0.87	0.76	0.82
10 - 50 hPa	0.94	0.80	0.94

Table 3. Total column ozone (TCO) differences in DU between AIRS, OMI and ozonesonde, during twelve months.

TCO Diff. (DU)	Jan	Feb	Mar	Apr	May	Jun	Jul	Aug	Sep	Oct	Nov	Dec
AIRS-OMI	-3.9	2.2	-1.8	13.2	16.7	18	-2.2	17.2	22.1	13.2	0.0	-2.7
AIRS-ozonesonde	-2.1	3.5	6.0	8.1	19.4	11.8	-2.3	22.3	21.6	15.0	5.6	5.2

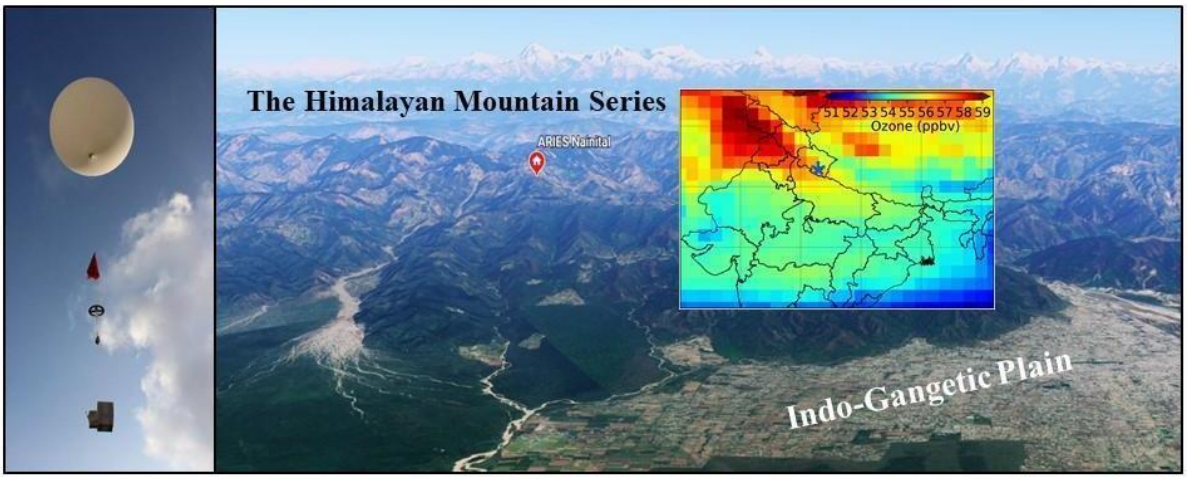

Figure 1. Location (red color circle) of the balloon launching site (© Google Earth, 2021) situated in the Aryabhatta Research Institute of Observational Sciences (ARIES) (29.4^{o} N, 79.5^{o} E, and 1793 m elevation), Nainital in the central Himalaya. The spatial distribution of ozone (AIRS) at 500 hPa is also shown over northern India and the location of the site is marked with a blue star. A photo of balloon, together with parachute, unwinder, ozonesonde along with GPS-radiosonde above the observation site is also shown at the left.

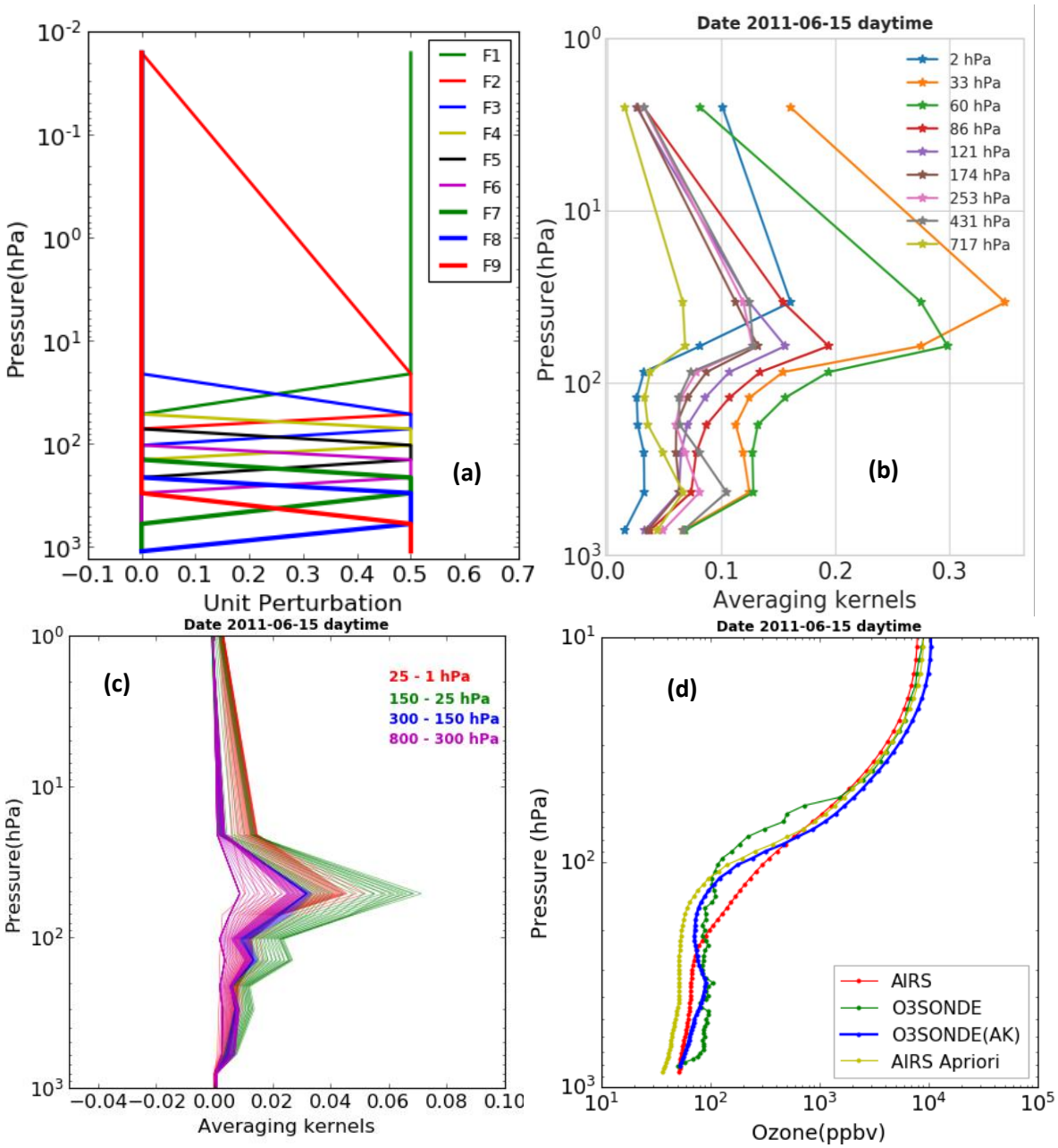

Figure 2. (a) Nine trapezoid functions used for ozone retrieval in AIRS-V6. (b) AIRS ozone averaging kernel matrix over Nainital at 9 levels vertical grid. (c) Calculated AIRS averaging kernel matrices at 100 RTA grids after applying the trapezoid function. (d) An example of ozone profiles using different data sets for 15 June, 2011 over the observation site.

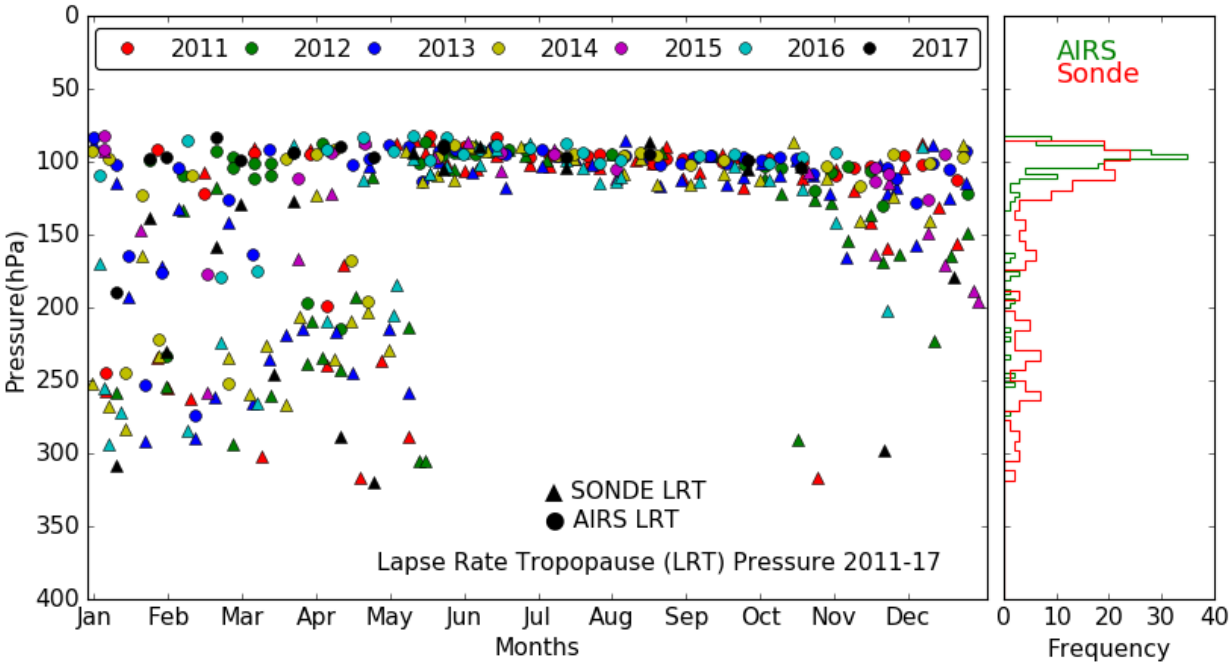

Figure 3. Lapse rate tropopause pressure monthly variation from balloon-borne and AIRS observations and respective frequency distributions during 2011 - 2017.

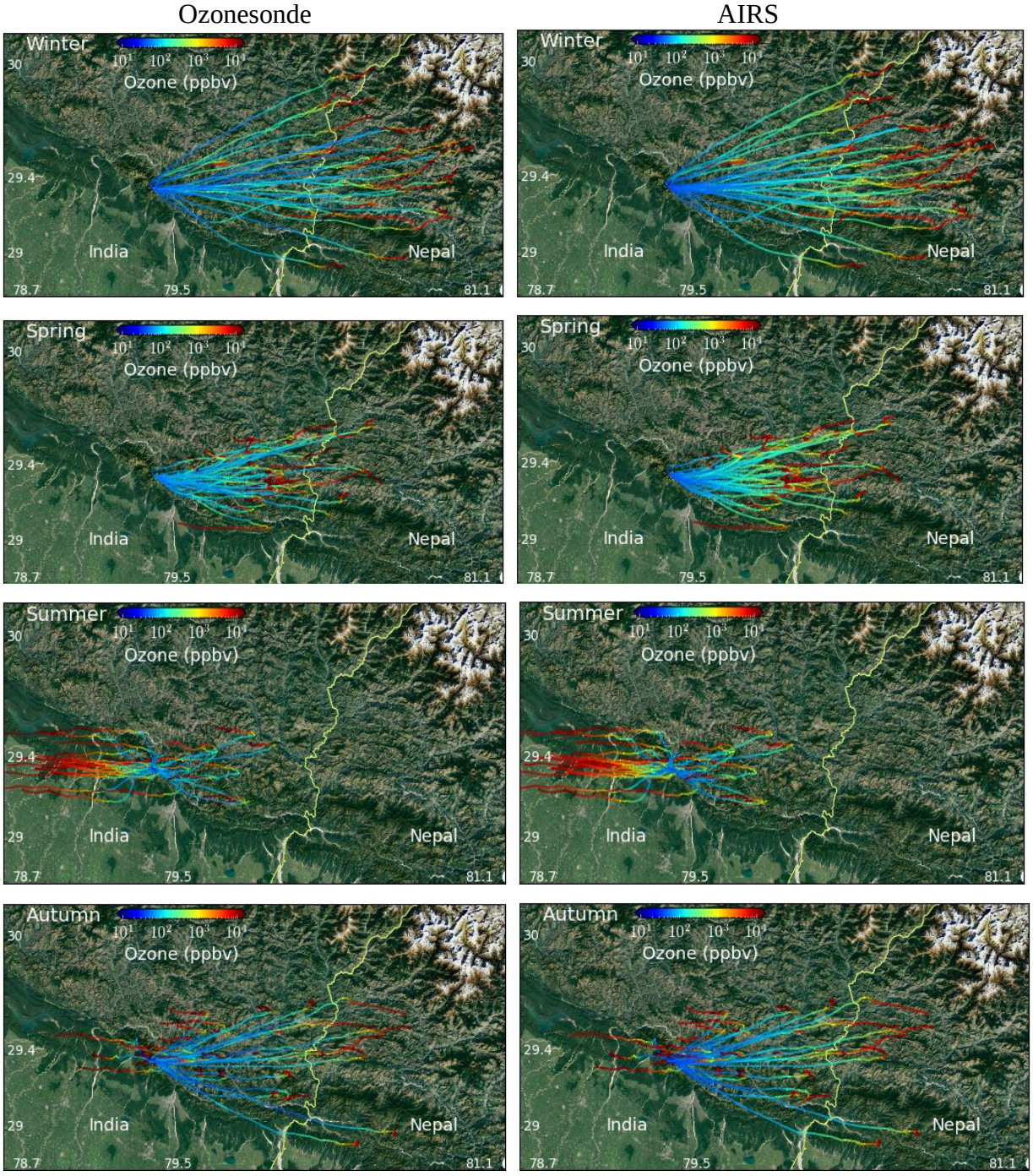

Figure 4. Spatial distribution of ozone using all ozone soundings (left) launched from ARIES, Nainital, India (© Google Earth, 2021) along with the balloon trajectories. Ozone spatial distribution from AIRS (right), following the balloon tracks, is also shown. It could be seen that the balloon reaches Nepal many times in the autumn and winter seasons.

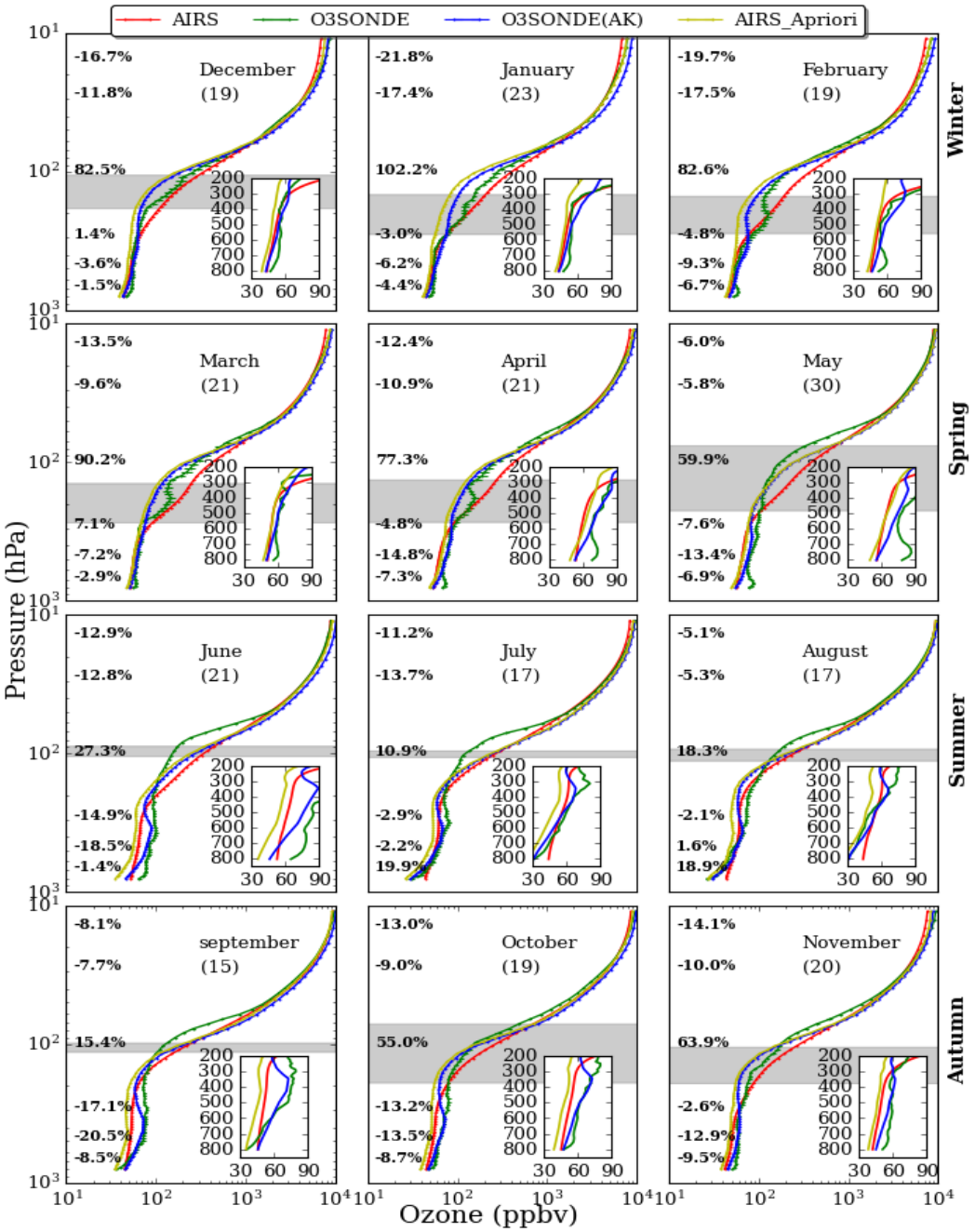

Figure 5. Monthly averaged (2011-2017) ozone profiles of ozonesonde, AIRS, ozonesonde (AK) and AIRS a-priori over Nainital in the central Himalaya. The percentage difference [(AIRS – ozonesonde (AK))/ozonesonde (AK)]*100 at 706, 496, 300, 103, 29, and 14.4 hPa are also written at respective altitudes. The standard error corresponding to each profile is also shown with error bars. The number of ozonesonde for different months is written in the bracket and grey shaded area shows the tropopause (mean ± sigma) from balloon-borne observations.

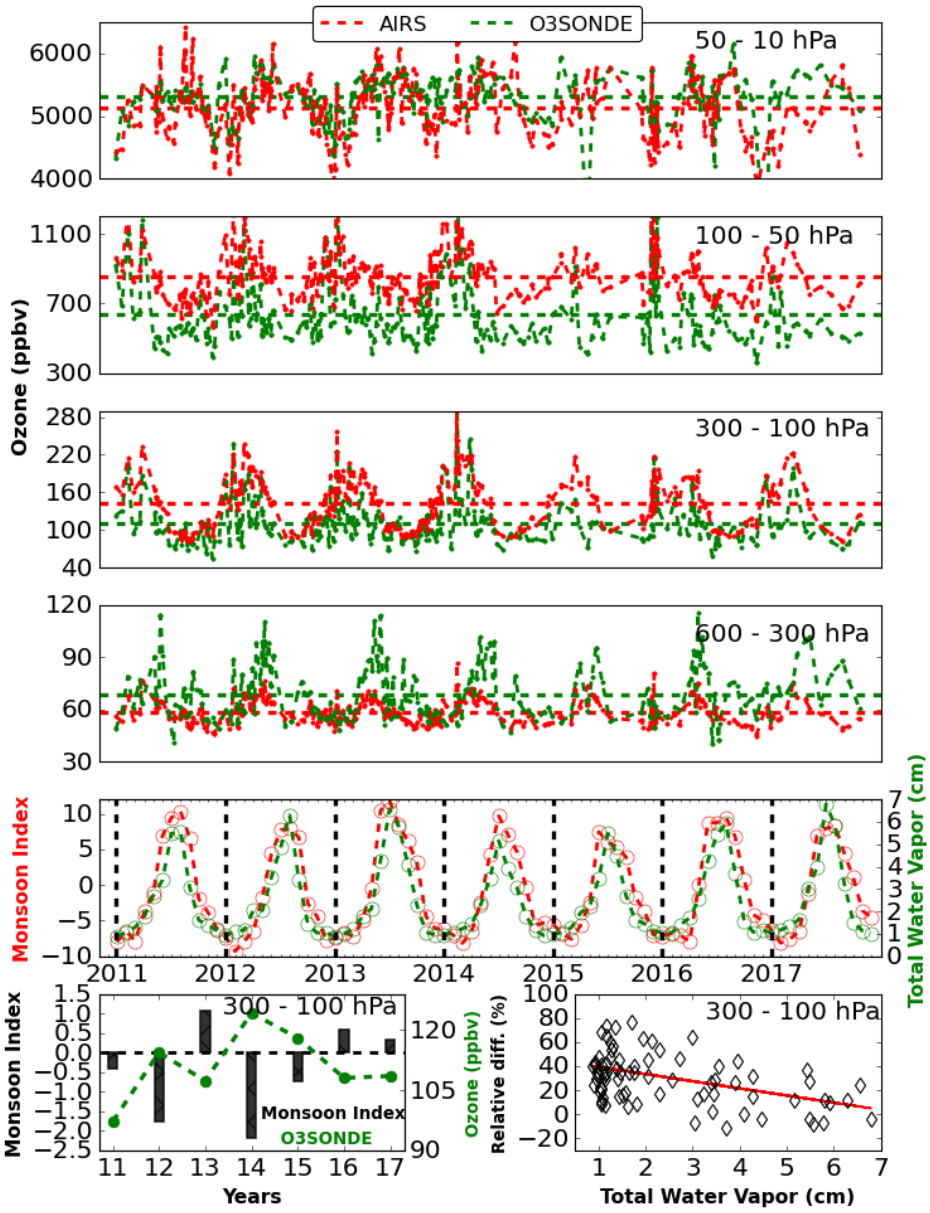

Figure 6. Average variations in ozone mixing ratios at four defined layers, characterizing the middle stratosphere (50 - 10 hPa), the lower stratosphere (100 - 50 hPa), the upper troposphere (300 - 100 hPa), and the middle troposphere (600 - 300 hPa), respectively. The red and green dash horizontal lines show the average ozone mixing ratios in the defined layers from AIRS and ozonesonde, respectively, from 2011 to 2017. The monthly variation of the total column water vapor (cm) along with the monsoon index is also shown. The yearly average ozone from ozonesonde and monsoon index (bar plot) for different years (left lower most) and scattered plot of ozone relative difference (%) [(AIRS-O3SONDE)/O3SONDE]*100, with total water vapor (right lower most) in the upper troposphere (300 - 100 hPa) are also shown.

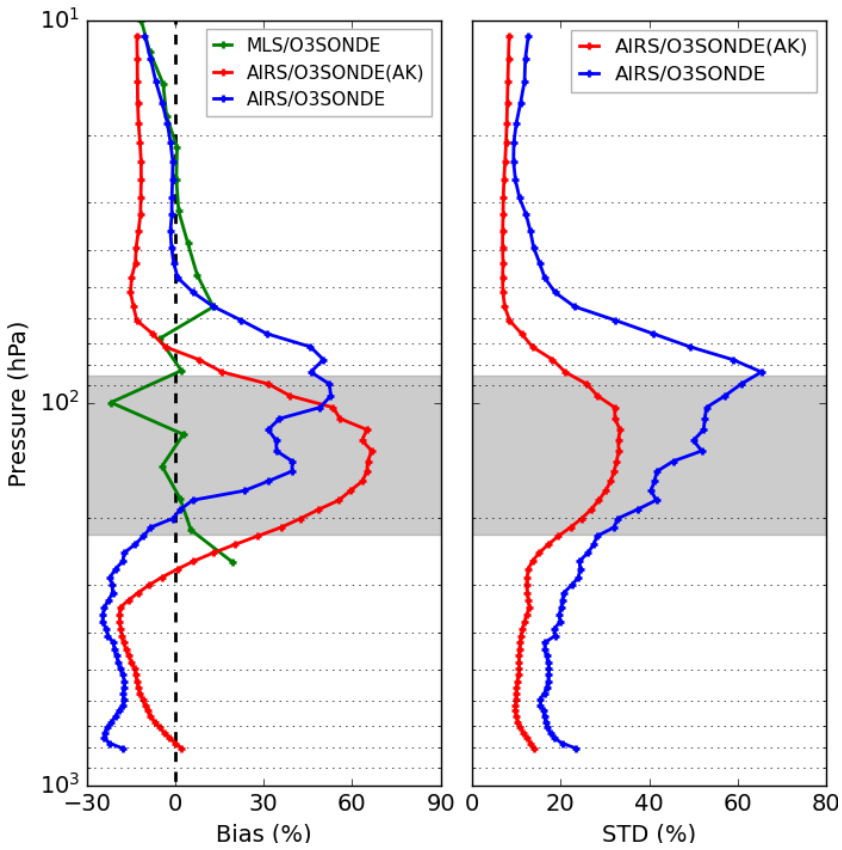

1252

1253 **Figure 7.** Statistical error analysis (Bias and standard deviation) of AIRS retrieved ozone with
1254 ozonesonde and ozonesonde (AK) for collocated data of seven years (2011 - 2017). The Bias
1255 between collocated data of MLS (261 hPa - 10 hPa) and ozonesonde over Nainital during 2011 -
1256 2017 is also shown with the green profile. The grey shaded area shows the tropopause region from
1257 balloon-borne radiosondes observations.

1258

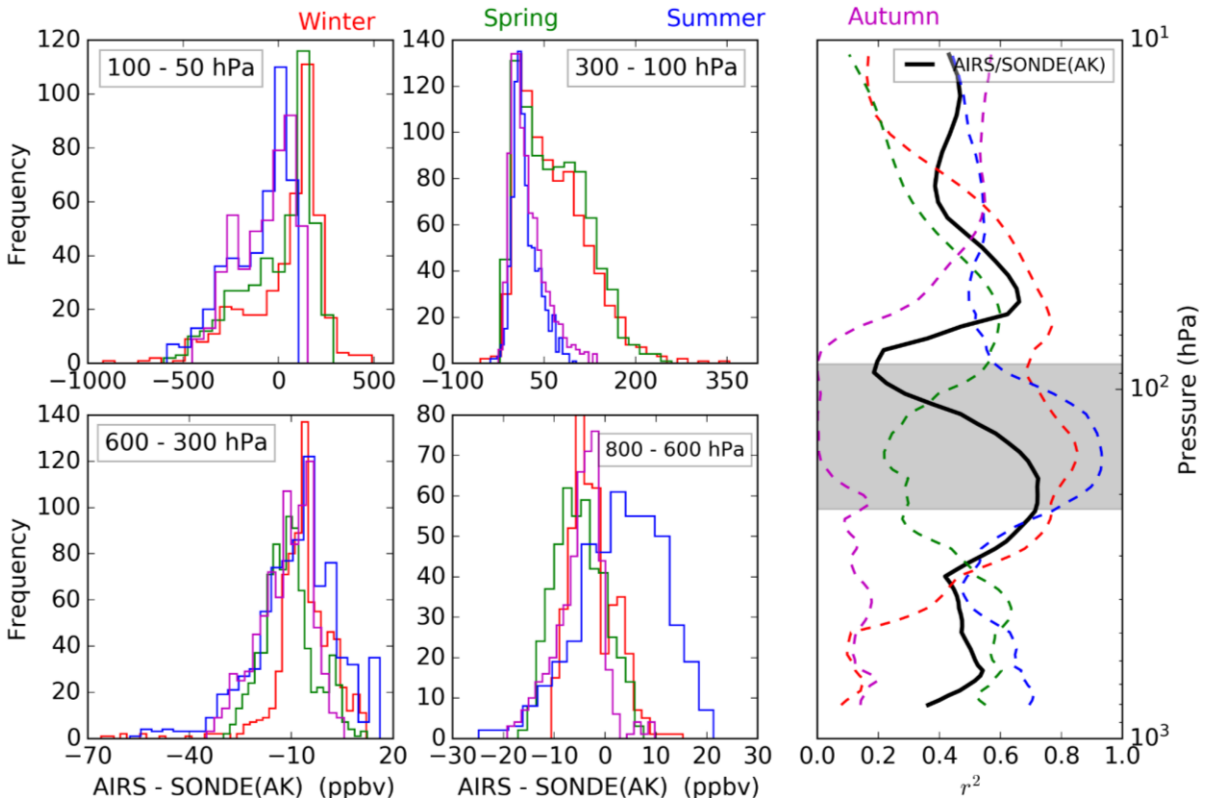

1259

1260 **Figure 8.** Histogram difference between AIRS ozone and ozonesonde (AK) in the four defined

1261 layers. The average correlation profiles between AIRS ozone and ozonesonde (AK) are shown on

1262 the right during winter (red), spring (green), summer-monsoon (blue), and autumn (magenta). The

1263 black line is for the entire data set. The grey shaded area shows the tropopause region from balloon-

1264 borne radiosondes observations.

1265

1266

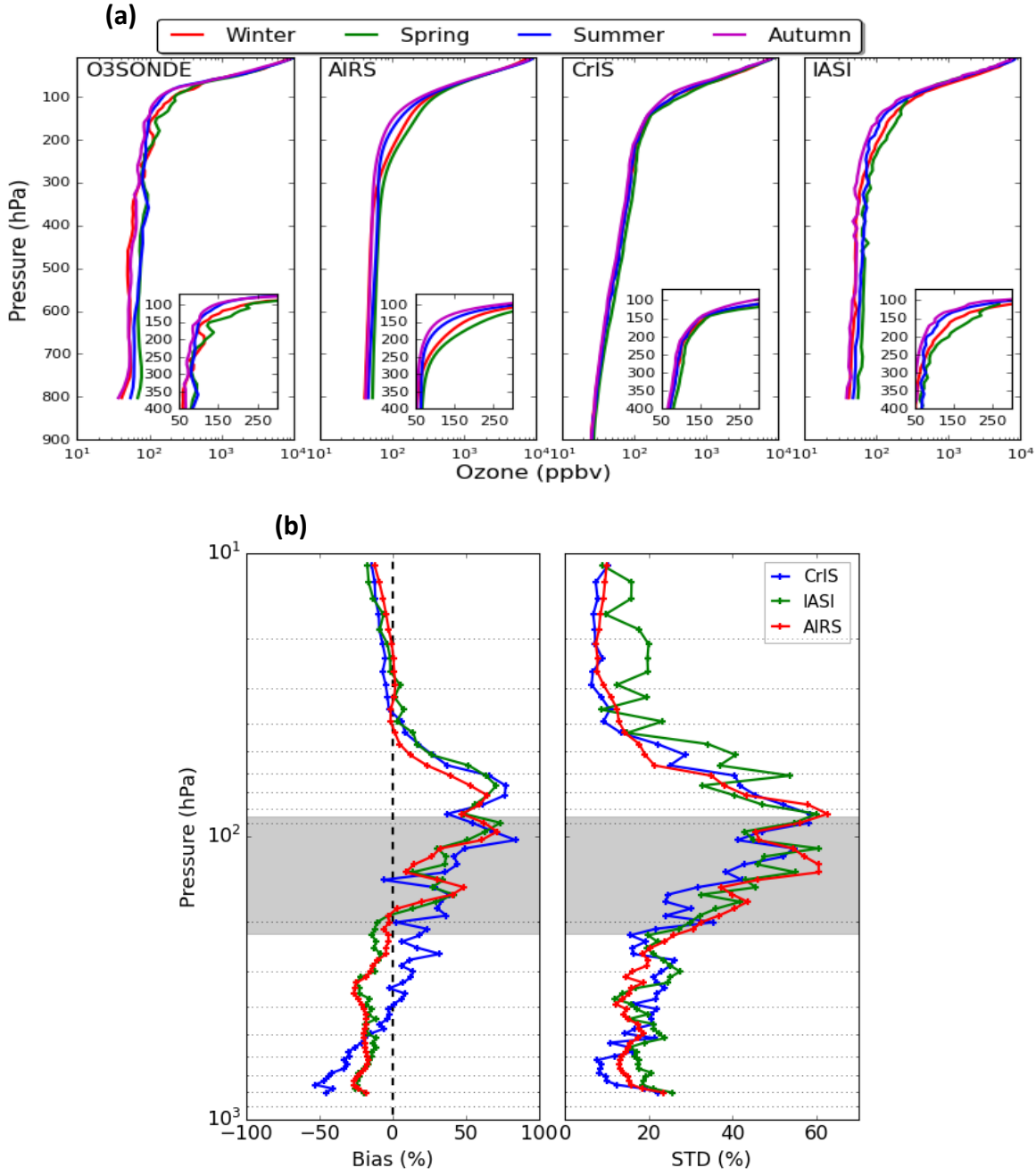

Figure 9. (a) Seasonal ozone profiles of three IR satellites (IASI, AIRS, and CrIS) for a smaller sample size (April 2014 to April 2015). The IASI and CrIS products are generated using the AIRS heritage algorithm (NOAA) and only zero quality flags (QC=0) of retrieval are used. (b) Statistical error analysis for the three IR satellites retrieved ozone without applying the averaging kernel information. The grey shaded area shows the tropopause region from balloon-borne observations.

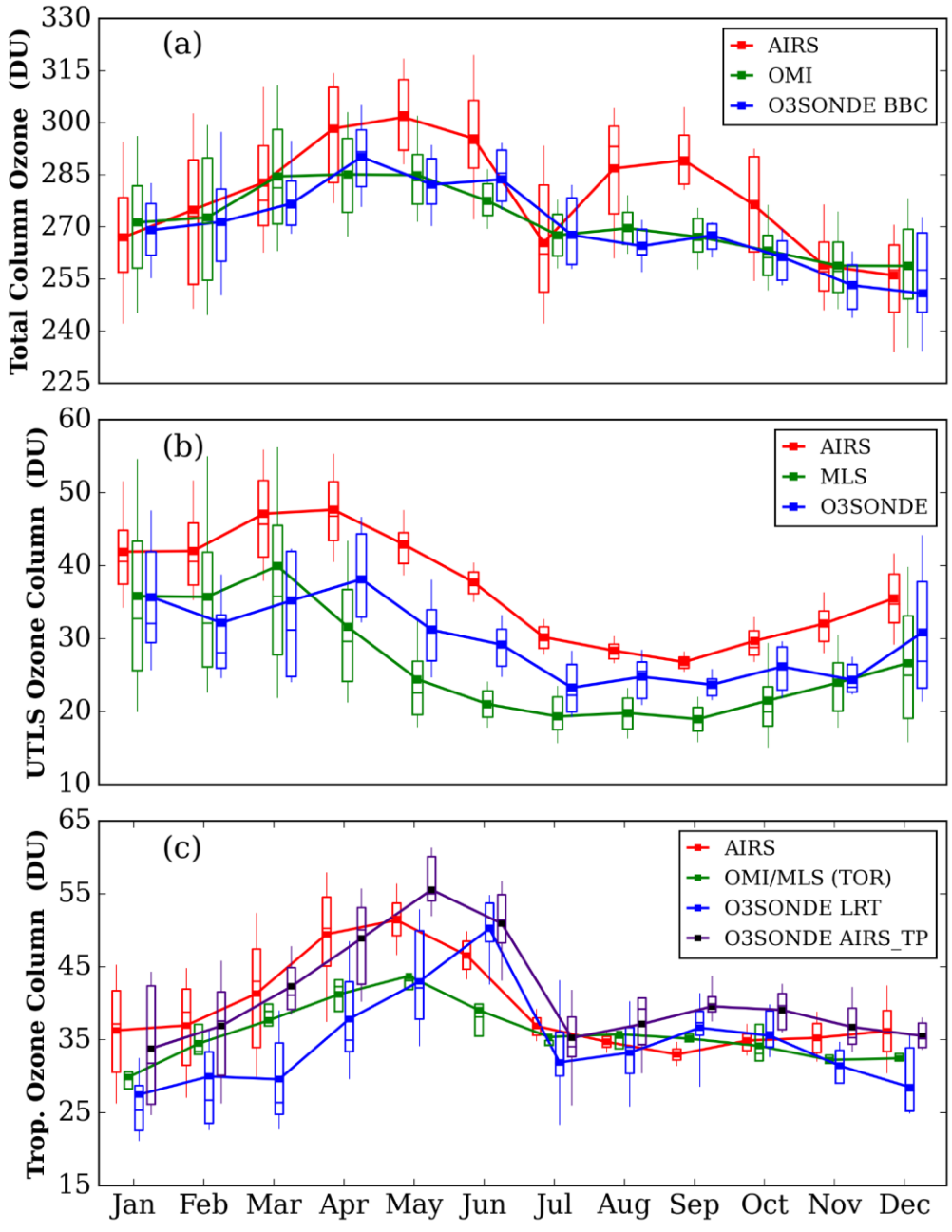

Figure 10. (a) Monthly average variations of total column ozone (TCO) for AIRS, OMI, and ozonesonde (Balloon Burst Climatology) over the central Himalaya for the 2011-2017 period. (b) Monthly average variation of UTLS ozone column for AIRS, MLS, and ozonesonde, over the central Himalayas for the 2011-2017 period. (c) Monthly average variations of tropospheric ozone column of AIRS, OMI/MLS (Tropospheric Ozone Residual), and ozonesonde (LRT - sonde lapse rate) over the central Himalayas for the 2011-2017 period. The ozonesonde tropospheric ozone column is also shown using AIRS tropopause (AIRS_TP). In the box plot, the lower and upper edges of the boxes represent the 25th and 75th percentiles. The whiskers below and above are 10th and 90th percentiles.

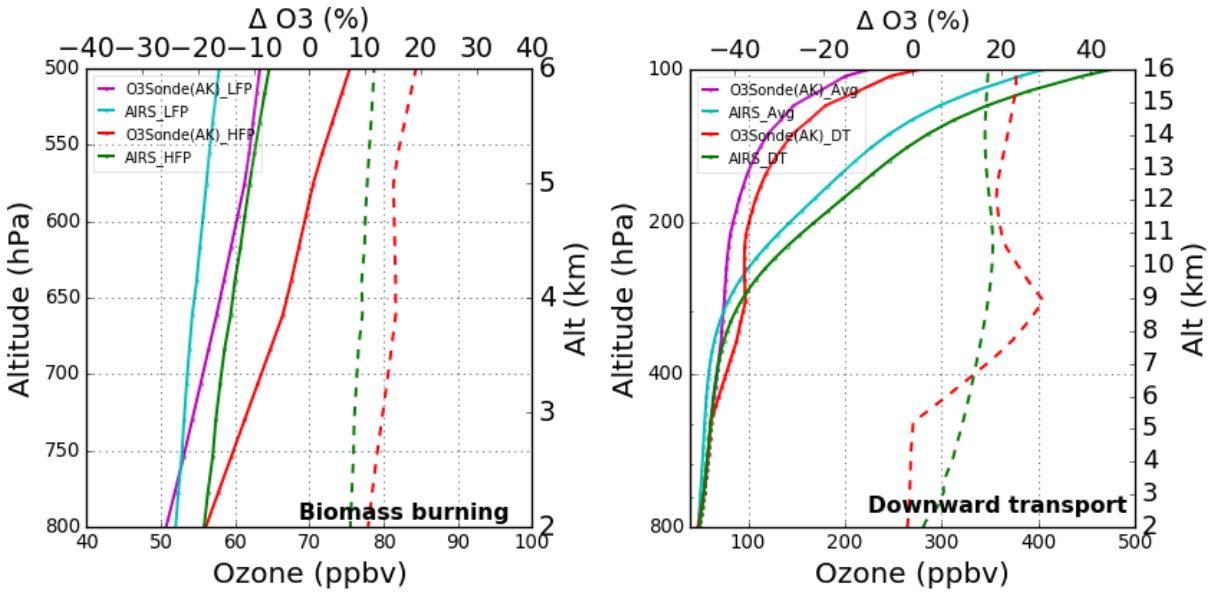

Figure 11. (a) Vertical ozone profiles of AIRS ozone and ozonesonde (AK) during low fire period (LFP) and high fire period (HEP). The solid lines correspond to ozone profiles while the dotted lines show a percentage increase in ozonesonde (red) and AIRS (green) profiles during biomass burning events. (b) Vertical ozone profiles of AIRS ozone and ozonesonde (AK) during events of downward transport. The dotted line shows ozone enhancement during downward transport events.

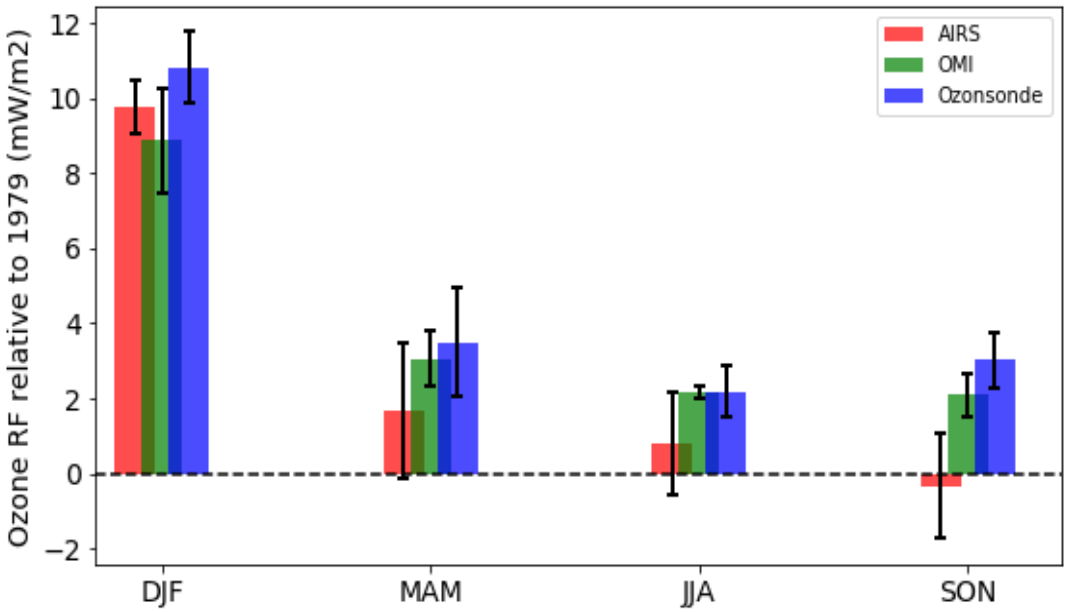

Figure 12. Seasonal average ozone UV radiative forcing (RF) relative to 1979 as calculated from ozonesonde, OMI, and AIRS total ozone data for the 2011 - 2017 period. Spreads correspond to one standard deviation.